109. S. Sternklar, S. Weiss, M. Segev, and B. Fischer, *Appl. Opt.* **25**, 4518 (1986).
110. Q. C. He, J. G. Duthie, and D. A. Gregory, *Opt. Lett.* **14**, 575 (1989).
111. S. Sternklar, S. Weiss, M. Segev, and B. Fischer, *Opt. Lett.* **11**, 528 (1986).
112. H. J. Caulfield, J. Shamir, and Q. He, *Appl. Opt.* **26**, 2291 (1987).
113. J. Shamir, H. J. Caulfield, and B. M. Hendrickson, *Appl. Opt.* **27**, 2912 (1988).
114. M. P. Schamshula, H. J. Caulfield, and C. M. Verber, *Opt. Lett.* **16**, 1421 (1991).
115. S. Weiss, M. Segev, S. Strenklar, and B. Fischer, *Appl. Opt.* **27**, 3422 (1988).
116. Q. He, J. Shamir, and J. G. Duthie, *Appl. Opt.* **28**, 306 (1989).
117. L. E. Adam and R. S. Bondurant, *Opt. Lett.* **16**, 832 (1991).
118. M. Petrov, E. U. Mokrushina, and H. J. Caulfield, unpublished data.

LASER AND PULSED-LASER NMR SPECTROSCOPY

M. W. EVANS*

Cornell Theory Center, Cornell University, Ithaca, NY
and
Materials Research Laboratory, The Pennsylvania State University, University Park, PA

CONTENTS

*Present address: Department of Physics, University of North Carolina, Charlotte, NC 28223.

Modern Nonlinear Optics, Part 2, Edited by Myron Evans and Stanisław Kielich. Advances in Chemical Physics Series, Vol. LXXXV.
ISBN 0-471-57546-1

I. INTRODUCTION

It was realized soon after the first demonstration of lasing action that circularly polarized electromagnetic radiation can produce bulk magnetization. Pershan and coworkers developed the effect theoretically[1] and experimentally,[2-4] and named it the inverse Faraday effect. Thereafter, Kielich[5, 6] produced a general theory of the relevant magneto-optics in terms of molecular property tensors, and Atkins and Miller[7] extended the theoretical considerations with quantum field theory. This important work has in common the induction by a circularly polarized laser of an electronic magnetic dipole moment ($m_i^{(\mathrm{ind})}$) in the atom or molecule under consideration

$$m_i^{(\mathrm{ind})} = \tfrac{1}{4}{}^{m}\chi_{ijk}^{\mathrm{ee}}(0;\omega,-\omega)E_j(\omega)E_k^*(\omega) \tag{1}$$

Here ${}^{m}\chi_{ijk}^{\mathrm{ee}}(0;\omega,-\omega)$ is the relevant susceptibility tensor,[8-10] and $E_jE_k^*$ is the tensor product of the electric field vector of the laser (in volts per meter) with its complex conjugate $\mathbf{E}^*$. Later, Manakov et al.[8-10] developed the general quantum structure of the susceptibility in Eq. (1) between eigenstates of different magnetic quantum number M. In this quantum theory, worked out analytically for atoms, the mean value of the permanent electronic magnetic dipole moment operator is

$$\mathbf{m}_0 = \langle JM|\hat{m}_0|JM'\rangle \equiv \langle \psi_m(t)|\hat{m}_0|\psi_{m'}(t)\rangle \tag{2}$$

where ψ_m and $\psi_{m'}$ are solutions of the Schrödinger equation corresponding to the initial and final atomic eigenstates $|JM\rangle$ and $|JM'\rangle$, both of which are M-fold degenerate. The initial and final eigenstates correspond in general therefore to different projections of M, i.e., different spatial quantization. The total electronic magnetic dipole moment in the presence of the laser can therefore be expressed as

$$\mathbf{m} = \mathbf{m}_0 + \mathbf{m}^{(\mathrm{ind})} = \langle JM|\hat{m}_0|JM'\rangle + \tfrac{1}{4}{}^{m}\chi_{ijk}^{\mathrm{ee}}E_jE_k^* \tag{3}$$

to order two in $\mathbf{E}$. The susceptibility also depends on M and M', and must therefore be spatially quantized. The induced magnetic dipole moment $\mathbf{m}^{(\mathrm{ind})}$ of Eq. (1) is therefore also spatially quantized when there is M degeneracy of this type. This is an important point in second-order laser NMR effects, because it means that the laser-induced electronic magnetic dipole moment $\mathbf{m}^{(\mathrm{ind})}$ can couple within the framework of quantum angular momentum theory[11-14] with the permanent nuclear magnetic dipole moment to shift and split existing NMR resonance lines, leading to a new spectral fingerprint. The same is true of second-order effects in laser ESR. The J and M quantization structure of the susceptibility ${}^{m}\chi_{ijk}^{\mathrm{ee}}$ of the inverse Faraday effect is given by Manakov et al.[8-10] in atoms when net electronic angular momentum. The interested reader is referred to Eq. (5.7), p. 607, of Ref. 9 for details. The quantization structure of the induced magnetic dipole moment of Eq. (1) for these atoms is clearly the same, and quantum transitions are allowed between M states governed by selection rules determined by the symmetry of the susceptibility tensor.

When there is M degeneracy, therefore, the induced electronic magnetic dipole moment of the inverse Faraday effect is spatially quantized, its expectation value depends explicitly on M and J through the Wigner-Eckart theorem,[8-10] and the induced magnetic dipole operator is proportional to a quantum mechanical electronic angular momentum operator, which can couple with another quantized nuclear or electronic angular momentum to produce spectral shifting and splitting in laser NMR and ESR.

II. FIRST-ORDER EFFECT IN LASER NMR

The theories mentioned in the introduction do not deal with an important first-order interaction energy that is dominant[14-18] in laser NMR. This first-order interaction will be developed before we return to second-order effects. The origin of this interaction energy can be found in the antisymmetric part of the tensor product $E_iE_j^*$:

$$\mathrm{antisym}(E_iE_j^*) = \tfrac{1}{2}(E_iE_j^* - E_jE_i^*) \tag{4}$$

which can be written as the vector cross-product

$$\mathbf{\Pi}^{(\mathrm{A})} = \mathbf{E}\times\mathbf{E}^* = \pm 2E_0^2 i\mathbf{k} \tag{5}$$

the antisymmetric conjugate product of a circularly polarized laser. It has been shown elsewhere[19] that $\mathbf{\Pi}^{(\mathrm{A})}$ is negative to motion reversal symmetry (T), is positive to parity inversion (P), is an axial vector, and changes sign when the circular polarity (handedness) of the laser is switched from left to right. The IUPAC standard expressions for $\mathbf{E}$ and $\mathbf{E}^*$ are (Appendix A)

$$\begin{aligned} \mathbf{E}_{\mathrm{L}} &= E_0(\mathbf{i}+\mathrm{i}\mathbf{j})\exp(-\mathrm{i}\phi_{\mathrm{L}}) & \mathbf{E}_{\mathrm{L}}^* &= E_0(\mathbf{i}-\mathrm{i}\mathbf{j})\exp(\mathrm{i}\phi_{\mathrm{L}}) \\ \mathbf{E}_{\mathrm{R}} &= E_0(\mathbf{i}-\mathrm{i}\mathbf{j})\exp(-\mathrm{i}\phi_{\mathrm{R}}) & \mathbf{E}_{\mathrm{R}}^* &= E_0(\mathbf{i}+\mathrm{i}\mathbf{j})\exp(\mathrm{i}\phi_{\mathrm{R}}) \end{aligned} \tag{6}$$

and from these definitions:

$$\mathbf{E}_L \times \mathbf{E}_L^* = -\mathbf{E}_R \times \mathbf{E}_R^* = -2E_0^2 \mathbf{i}\mathbf{k} \tag{7}$$

a purely imaginary quantity. It is important to note that $\mathbf{k}$ in this equation is a P-positive, T-negative, unit axial vector in the propagation axis of the circularly polarized laser, denoted Z, and should not be confused with the propagation vector of the laser (denoted $\boldsymbol{\kappa}$), which is negative to P and T.[20] In Eq. (7), E_0 is the scalar electric field strength amplitude of the laser in volts per meter. Clearly, if the laser is linearly polarized, it is 50% right and 50% left circularly polarized, and $\mathbf{\Pi}^{(A)}$ vanishes.

Using the fundamental electrodynamical relations

$$I_0 = \tfrac{1}{2}\varepsilon_0 c E_0^2 \tag{8}$$

and

$$E_0 = cB_0 \tag{9}$$

where B_0 is the scalar magnetic flux density amplitude of the laser in tesla, c is the speed of light (a scalar), I_0 is the laser's scalar intensity in watts per square meter, and

$$\varepsilon_0 = 8.854 \times 10^{-12} J^{-1} C^2 m^{-1} \tag{10}$$

is the scalar permittivity in vacuo in S.I. units, the vector $\mathbf{\Pi}^{(A)}$ can be rewritten as

$$\mathbf{\Pi}^{(A)} = \left(\frac{8I_0 c}{\varepsilon_0}\right)^{1/2} (\pm B_0 \mathbf{k})\mathbf{i} \tag{11}$$

which is proportional to the product of B_0 and $\mathbf{k}$ through a T- and P-positive scalar quantity. The product

$$\mathbf{B}_\Pi = B_0 \mathbf{k} \tag{12}$$

is the laser's equivalent static magnetic flux density vector, because (1) it has the units of magnetic flux density (tesla), and (2) it has the correct fundamental symmetries of magnetic flux density, being a T-negative, P-positive axial vector. We therefore arrive at the important relations

$$\mathbf{\Pi}^{(A)} = \mathbf{i}\left(\frac{8I_0 c}{\varepsilon_0}\right)^{1/2} (\pm \mathbf{B}_\Pi) \tag{13}$$

and

$$|\mathbf{B}_\Pi| = B_0 = \left(\frac{2I_0}{\varepsilon_0 c^3}\right)^{1/2} \tag{14}$$

between $\mathbf{\Pi}^{(A)}$ and $\mathbf{B}_\Pi$ of a circularly polarized laser, and find that such a laser generates a static magnetic field $\mathbf{B}_\Pi$ in its propagation axis. Since $\mathbf{B}_\Pi$ is negative to motion reversal T, it must change sign if the motion of the laser is reversed, i.e., if the laser is made to propagate in the opposite direction in Z. However, $\mathbf{B}_\Pi$ is positive to parity inversion P because the conjugate product $\mathbf{\Pi}^{(A)}$ is positive to P:

$$P(\mathbf{E}) = -\mathbf{E} \qquad P(\mathbf{E}^*) = -\mathbf{E}^* \qquad P(\mathbf{E} \times \mathbf{E}^*) = \mathbf{E} \times \mathbf{E}^* \tag{15}$$

confirming that $\mathbf{\Pi}^{(A)}$ and $\mathbf{B}_\Pi$ have the same fundamental symmetries and are both axial vectors, proportional to each other through a T- and P-positive scalar quantity. It is important to note that the conjugate product $\mathbf{\Pi}^{(A)}$ changes sign with circular polarity of the laser and so does $\mathbf{B}_\Pi$. The origin of the sign change in $\mathbf{\Pi}^{(A)}$ in this context is neither the operation P nor T, but the different operation $(\hat{H})$ on the components $\mathbf{E}$ and $\mathbf{E}^*$ (Appendix A):

$$\left[E_L = E_0(\mathbf{i} + \mathbf{i}\mathbf{j})e^{-i\phi_L}\right] \xrightarrow{\hat{H}} \left[\mathbf{E}_R = E_0(\mathbf{i} - \mathbf{i}\mathbf{j})e^{-i\phi_R}\right]$$

an operation that switches the laser from left to right circular polarization (c.p.). In a left c.p. laser, $\mathbf{\Pi}^{(A)}$ is formed by multiplying $-\mathbf{B}_\Pi$, and in a right c.p. laser, it is formed by multiplying $+\mathbf{B}_\Pi$.

We conclude that a circularly polarized laser can act as a light magnet, generating a static magnetic flux density $\pm\mathbf{B}_\Pi$ in the axis of propagation. This is of key importance to the first-order effect of such a laser on NMR spectra, and probably also to many other effects, because a circularly polarized laser can always be used as a magnet, and a magnet is used in many interesting investigations.

For I_0 of 10 000 W/m^2 (1.0 W/cm^2)

$$\mathbf{B}_\Pi \doteqdot 10^{-5}\,\mathbf{k}\,\mathrm{T} \tag{16}$$

and the equivalent magnetic flux density of the laser is 10^{-5} T. Pulsed lasers can deliver up to 10^{16} W/m^2 (Ref. 20) over subpicosecond time intervals, delivering 10.0 T. This is about the same order of magnitude as the most powerful contemporary superconducting magnets.

Since $\mathbf{B}_\Pi$ is a real static magnetic flux density, it forms a T- and P-positive scalar interaction energy with a nuclear magnetic dipole moment $\mathbf{m}^{(N)}$. This is the key to laser and pulsed laser NMR spectroscopy, because this is the big, first-order mechanism. Note that in this context we have defined $\mathbf{m}^{(N)}$ to be a real axial vector, T negative and P positive. The quantum-mechanical nuclear magnetic dipole moment operator $\hat{\mathbf{m}}^{(N)}$ has the same symmetries, but is a purely imaginary quantity.[21] Therefore, $\mathbf{m}^{(N)}$ is to be regarded as the real observable generated by the operator $\hat{\mathbf{m}}^{(N)}$. The interaction energy

$$E_1 = -\mathbf{m}^{(N)} \cdot \mathbf{B}_\Pi \tag{17}$$

is quantized, in the same way as the usual interaction energy generated by $\mathbf{m}^{(N)}$ and the static magnetic flux density $\mathbf{B}_0$ of the big permanent magnet of an NMR spectrometer.

If we now direct a circularly polarized laser parallel to $\mathbf{B}_0$, the combined interaction energy becomes

$$E_2 = -\mathbf{m}^{(N)} \cdot (\mathbf{B}_0 \pm \mathbf{B}_\Pi) \tag{18}$$

i.e., the original NMR resonance frequency is shifted by the laser by an amount

$$\Delta f = \pm(\mathbf{m}^{(N)} \cdot \mathbf{B}_\Pi)/h \tag{19}$$

in hertz, where h is Planck's constant. It turns out (vide infra) that experimentally such a shift is site specific, i.e., the shift is different for each resonating nucleus, essentially because the $\mathbf{B}_\Pi$ at the nucleus is different from the applied $\mathbf{B}_\Pi$ due to the well-known chemical shift effect, and this leads to a valuable new fingerprint of a complex system such as a folded protein in solution.[22-30]

A. Bulk Magnetization Due to $\mathbf{B}_\Pi$: Comparison with Data

It is useful as a check to calculate the order of magnitude of magnetization $\mathbf{M}_\Pi$ (in amps per meter) expected from a laser delivering $\mathbf{B}_\Pi$ in tesla, and to compare this with experimental data. The basic relation between $\mathbf{M}_\Pi$ and $\mathbf{B}_\Pi$ is given by Atkins[31]:

$$\mathbf{M}_\Pi = \frac{1}{\mu_0}\left(\frac{\kappa_m}{1+\kappa_m}\right)\mathbf{B}_\Pi \tag{20}$$

where κ_m is the dimensionless mass susceptibility of the sample, and μ_0 is the permeability in vacuo,

$$\mu_0 = 4\pi \times 10^{-7} NA^{-2} \tag{21}$$

Atkins gives a useful model calculation for an ensemble of atoms with and without net electronic spin. In the latter case (Ref. 31, Eq. (14.2.27a)),

$$\kappa_m = -\frac{e^2\mu_0}{6m_e} N\langle r^2\rangle \tag{22}$$

where e is the electronic charge, N the number density (atoms per cubic meter), m_e the mass of the electron, and $\langle r^2\rangle$ is about 10^{-20} m^2. For a model atomic weight of 20, this gives a mass susceptibility of the order 2×10^{-9} and a magnetization from Eq. (20) of the order 10^{-5} A/m for $\mathbf{B}_\Pi$ of 0.03 T. The latter is derived using Eq. (14) from the peak intensity of 10^{11} W/m^2 recorded by Pershan et al.,[2-4] who observed a magnetization of the order 10^{-5} G (10^{-2} A/m) in 3.1% Eu^{2+}-doped calcium fluoride glass due to a circularly polarized giant ruby laser pulse of 30 ns. The calculated figure is therefore about 300 times smaller than the experimental one, but the experimental sample was paramagnetic, whereas Eq. (22) is for a diamagnetic atomic sample. Furthermore, the effective molecular weight of the doped glass sample is greater than 20, and Pershan et al.[2-4] observed a dominant paramagnetic contribution that was temperature dependent. Following the argument on p. 386 of Atkins,[31] the magnetization for one gram of sample with unpaired spin (such as Na) will be of the order 1000 times bigger. This argument leads to a calculated magnetization $\mathbf{M}_\Pi$ fortuitously of the same order of magnitude as that observed by Pershan et al.[2-4]

The concept of equivalent static magnetic flux density leads to a reasonable description of the only available data in the literature on magnetization by a circularly polarized laser pulse. This estimate is dominated, however, by electronic mass susceptibility in a sample with net electronic angular momentum, and for optical NMR it is necessary to consider the interaction of $\mathbf{B}_\Pi$ with both nuclear and electronic spins in the sample. The existence of $\mathbf{B}_\Pi$ is the key to the fundamental interaction Hamiltonian at first order in optical NMR, and this is developed in the following section.

B. The Fundamental Equations of the First-Order Effect

Because $\mathbf{B}_\Pi$ is a static magnetic flux density, it is governed by fundamental equations from which the first-order optical NMR Hamiltonian can be constructed. The static magnetic flux density $\mathbf{B}_\Pi$ is related formally through

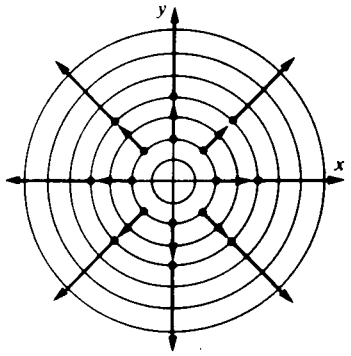

Figure 1. A vector potential with no curl. (Reprinted with permission from Ref. 31.)

a Maxwell equation with an electric field strength $\mathbf{E}_\Pi$:

$$\nabla \times \mathbf{E}_\Pi = -\frac{\partial \mathbf{B}_\Pi}{\partial t} = 0 \tag{23}$$

From this it is clear that $\mathbf{E}_\Pi$ has no curl, and must be a function of the type [31]

$$\mathbf{E}_\Pi = |\mathbf{E}_\Pi| k. \tag{24}$$

The vector potential ($\mathbf{A}_\Pi$) of $\mathbf{B}_\Pi$ is a radial flow in a plane perpendicular to the propagation axis of the laser (Figs. 1 and 2).

Having defined $\mathbf{E}_\Pi$ in this way, the equation of motion of one electron subjected to $\mathbf{B}_\Pi$ is given by the Lorentz force law

$$m_e \ddot{\mathbf{r}} = \mathbf{F}_\Pi = e(\mathbf{E}_\Pi + \dot{\mathbf{r}} \times \mathbf{B}_\Pi) \tag{25}$$

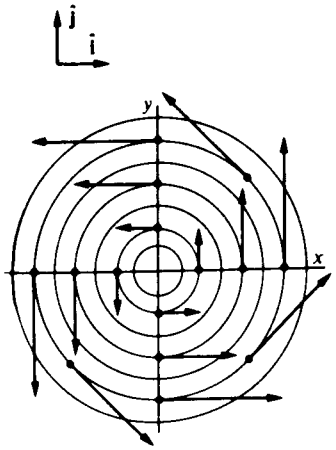

Figure 2. A vector potential with a nonzero curl. (Reprinted with permission from Ref. 31.)

where $\mathbf{r}$ is the position coordinate of the electron and m_e its mass. The Lorentz force equation (25) is equivalent to an Euler-Lagrange equation of motion with Lagrangian

$$L_\Pi = \tfrac{1}{2} m_e \dot{r}^2 + e\phi_\Pi - e\dot{\mathbf{r}} \cdot \mathbf{A}_\Pi \tag{26}$$

where ϕ_Π and $\mathbf{A}_\Pi$ are the scalar and vector potentials of the circularly polarized laser in the Lorentz gauge,[31] in which

$$\mathbf{B}_\Pi = \nabla \times \mathbf{A}_\Pi \qquad \mathbf{E}_\Pi = -\frac{\partial \mathbf{A}_\Pi}{\partial t} - \nabla\phi_\Pi \tag{27}$$

The vector potential $\mathbf{A}_\Pi$ of the circularly polarized laser in this gauge can be expressed as

$$\mathbf{A}_\Pi = \tfrac{1}{2}|\mathbf{B}_\Pi|\mathbf{V}_\Pi = \tfrac{1}{2}\mathbf{B}_\Pi \times \mathbf{r} \qquad \mathbf{V}_\Pi = -Y\mathbf{i} + X\mathbf{j} \tag{28}$$

and the curl of $\mathbf{V}_\Pi$ is twice the unit axial vector $\mathbf{k}$ defined previously by Eq. (5). It follows that the equivalent magnetic flux density $\mathbf{B}_\Pi$ of the circularly polarized laser is related to its vector potential $\mathbf{A}_\Pi$ by

$$\mathbf{B}_\Pi = \frac{B_0}{2}\nabla \times \mathbf{V}_\Pi = \nabla \times \mathbf{A}_\Pi \tag{29}$$

which is consistent with our earlier definitions.

The one-electron Hamiltonian in the presence of the circularly polarized laser can be found from the Hamiltonian in the absence of the laser

$$H^{(0)} = \frac{1}{2m_e} p^2 + \text{Potential energy} \tag{30}$$

by replacing the Newtonian momentum $\mathbf{p}$ by the generalized momentum[31]:

$$\mathbf{p}_\Pi = \mathbf{p} + e\mathbf{A}_\Pi \tag{31}$$

The transition from the classical to quantum-mechanical one-electron Hamiltonian in the presence of a c.p. laser is achieved by replacing the Newtonian momentum by the appropriate operator:

$$\mathbf{p}_\Pi \rightarrow -\mathrm{i}\nabla_\Pi \hbar = \hat{\mathbf{p}}_\Pi \tag{32}$$

With these equations the following are useful insights to the physical meaning of the conjugate product $\mathbf{E} \times \mathbf{E}^*$ (see also Appendix B).

1. The relation

$$\nabla \times \mathbf{A}_\Pi = \pm \frac{\mathrm{i}}{2}\left(\frac{\varepsilon_0}{2I_0 c}\right)^{1/2} (\mathbf{E} \times \mathbf{E}^*) \tag{33}$$

shows that the vector potential $\mathbf{A}_\Pi$ curls around the propagation axis of a circularly polarized laser.

2. On the Argand diagram $\mathbf{E}$ is perpendicular to its conjugate $\mathbf{E}^*$, and both vectors are rotating in the same direction at a fixed relative orientation. Their vector product is therefore mutually perpendicular (in the propagation axis) and is time independent, because the relative orientation of $\mathbf{E}$ and $\mathbf{E}^*$ does not change.

3. The P and T symmetries of the well-known Poynting vector[31]

$$\mathbf{N} = \mathbf{E} \times \mathbf{H}^* \doteqdot \frac{1}{\mu_0}\mathbf{E} \times \mathbf{B}^* \tag{34}$$

are not the same as that of the conjugate product $\mathbf{E} \times \mathbf{E}^*$. The Poynting vector measures the instantaneous energy flow in the direction of propagation of an electromagnetic wave, and is P- and T-negative. It has the same P and T symmetries as the propagation vector $\boldsymbol{\kappa}$ of a laser, and is a polar vector (one that changes sign with P). In contrast, the conjugate product $\boldsymbol{\Pi}^{(A)}$ and the $\mathbf{B}_\Pi$ vector are axial vectors, which do not change sign with P. It is important to make this distinction. Clearly, the Poynting vector cannot be a static magnetic flux density vector because of its negative P symmetry.

The reason for this is not straightforward. Consider the complete set of electromagnetic plane wave equations:

$$\begin{array}{lll}
\mathbf{E}_\mathrm{L} = E_0(\mathbf{i} + \mathrm{i}\mathbf{j})\mathrm{e}^{-\mathrm{i}\phi_\mathrm{L}} & P(\mathbf{E}_\mathrm{L}) = -\mathbf{E}_\mathrm{L} & T(\mathbf{E}_\mathrm{L}) = \mathbf{E}_\mathrm{R}^* \\
\mathbf{E}_\mathrm{R} = E_0(\mathbf{i} - \mathrm{i}\mathbf{j})\mathrm{e}^{-\mathrm{i}\phi_\mathrm{R}} & P(\mathbf{E}_\mathrm{R}) = -\mathbf{E}_\mathrm{R} & T(\mathbf{E}_\mathrm{R}) = \mathbf{E}_\mathrm{L}^* \\
\mathbf{E}_\mathrm{L}^* = E_0(\mathbf{i} - \mathrm{i}\mathbf{j})\mathrm{e}^{\mathrm{i}\phi_\mathrm{L}} & P(\mathbf{E}_\mathrm{L}^*) = -\mathbf{E}_\mathrm{L}^* & T(\mathbf{E}_\mathrm{L}^*) = \mathbf{E}_\mathrm{R} \\
\mathbf{E}_\mathrm{R}^* = E_0(\mathbf{i} + \mathrm{i}\mathbf{j})\mathrm{e}^{\mathrm{i}\phi_\mathrm{R}} & P(\mathbf{E}_\mathrm{R}^*) = -\mathbf{E}_\mathrm{R}^* & T(\mathbf{E}_\mathrm{R}^*) = \mathbf{E}_\mathrm{L} \\
\mathbf{B}_\mathrm{L} = B_0(\mathbf{j} - \mathrm{i}\mathbf{i})\mathrm{e}^{-\mathrm{i}\phi_\mathrm{L}} & P(\mathbf{B}_\mathrm{L}) = \mathbf{B}_\mathrm{L} & T(\mathbf{B}_\mathrm{L}) = -\mathbf{B}_\mathrm{R}^* \\
\mathbf{B}_\mathrm{R} = B_0(\mathbf{j} + \mathrm{i}\mathbf{i})\mathrm{e}^{-\mathrm{i}\phi_\mathrm{R}} & P(\mathbf{B}_\mathrm{R}) = \mathbf{B}_\mathrm{R} & T(\mathbf{B}_\mathrm{R}) = -\mathbf{B}_\mathrm{L}^* \\
\mathbf{B}_\mathrm{L}^* = B_0(\mathbf{j} + \mathrm{i}\mathbf{i})\mathrm{e}^{\mathrm{i}\phi_\mathrm{L}} & P(\mathbf{B}_\mathrm{L}^*) = \mathbf{B}_\mathrm{L}^* & T(\mathbf{B}_\mathrm{L}^*) = -\mathbf{B}_\mathrm{R} \\
\mathbf{B}_\mathrm{R}^* = B_0(\mathbf{j} - \mathrm{i}\mathbf{i})\mathrm{e}^{\mathrm{i}\phi_\mathrm{R}} & P(\mathbf{B}_\mathrm{R}^*) = \mathbf{B}_\mathrm{R}^* & T(\mathbf{B}_\mathrm{R}^*) = -\mathbf{B}_\mathrm{L}
\end{array} \tag{35}$$

The effect of P and T on each of these has been given explicitly, and to understand why the operators have the effect they do requires the following realization. The unit vectors $\mathbf{i}$ and $\mathbf{j}$ for the electric components are polar unit vectors that are T positive, P negative. Almost universally (and unfortunately), the same $\mathbf{i}$ and $\mathbf{j}$ notation is also used for the T-negative, P-positive, axial unit vectors of the magnetic components. However, the two sets of unit vectors denote quite different symmetries, which is revealed when we take the limit $\omega \to 0$, i.e., when the angular frequency of the wave is vanishingly small, so that the $\mathbf{E}$ and $\mathbf{B}$ vectors of the plane wave must become static electric field strength and magnetic flux density vectors. In this limit, the plane wave equations reduce to

$$\mathbf{E}_\mathrm{L} \xrightarrow{\omega \to 0} E_0(\mathbf{i} + \mathrm{i}\mathbf{j}) \text{ etc.} \qquad \mathbf{B}_\mathrm{L} \xrightarrow{\omega \to 0} B_0(\mathbf{j} - \mathrm{i}\mathbf{i}) \text{ etc.} \tag{36}$$

and the real parts must have the correct P and T symmetries of static $\mathbf{E}$ and $\mathbf{B}$. It follows that the unit vectors in the usual plane wave descriptions also have different fundamental symmetries, as described. From this the fundamental symmetries of the Poynting vector emerge as follows:

$$\begin{aligned}
P(\mathbf{E}_\mathrm{L} \times \mathbf{B}_\mathrm{L}^*) &= -(\mathbf{E}_\mathrm{L} \times \mathbf{B}_\mathrm{L}^*) \text{ etc.} \\
T(\mathbf{E}_\mathrm{L} \times \mathbf{B}_\mathrm{L}^*) &= -(\mathbf{E}_\mathrm{R}^* \times \mathbf{B}_\mathrm{R}) \\
&= -(\mathbf{E}_\mathrm{L} \times \mathbf{B}_\mathrm{L}^*) \text{ etc.}
\end{aligned} \tag{37}$$

It is important to realize that the equivalent magnetic flux density vector $\mathbf{B}_\Pi$, introduced in this chapter, is fundamentally different from the Poynting vector and propagation vector. For example, the latter two exist in linearly polarized radiation, because

$$\mathbf{E}_\mathrm{L} \times \mathbf{B}_\mathrm{L}^* = \mathbf{E}_\mathrm{R} \times \mathbf{B}_\mathrm{R}^* \tag{38}$$

while $\mathbf{B}_\Pi$ vanishes.

Having been careful to make these key distinctions, it is now possible to develop the first-order interaction Hamiltonian of optical NMR from an argument parallel with that given by Atkins,[31] for example:

$$H = H^{(0)} + H^{(1)} + H^{(2)} \tag{39}$$

where the first-order term is

$$H^{(1)} = -\gamma_\mathrm{e}\mathbf{B}_\mathrm{II} \cdot \mathbf{L} \tag{40}$$

with $\mathbf{L}$ denoting the orbital angular momentum, and γ_e the electronic

gyromagnetic ratio, and the second-order term is (see also Appendix B)

$$H^{(2)} = \frac{e^2}{8m_e} B_{\Pi}^2 (X^2 + Y^2) = \frac{e^2}{2m_e} A_{\Pi}^2 \tag{41}$$

This is a nonrelativistic treatment, so that the electronic spin component in Eq. (40) is missing. Reinstating the spin term leads to the familiar-looking first-order Hamiltonian describing the interaction between $\mathbf{B}_{\Pi}$ and an electronic magnetic dipole moment.

An entirely analogous procedure leads to the first-order Hamiltonian describing the interaction between $\mathbf{B}_{\Pi}$ and a nuclear magnetic dipole moment $\mathbf{m}^{(N)}$ and this has the same form as the right side of Eq. (17). It becomes clear, therefore, that the equations of conventional NMR, which use, for example, a homogeneous superconducting magnet to deliver a static $\mathbf{B}_0$ of up to 20.0 T, can be adapted easily for use with laser and pulsed-laser NMR using the new concept of $\mathbf{B}_{\Pi}$ (Appendix C).

III. CONTINUOUS-WAVE LASER NMR, OR LASER-ENHANCED NMR SPECTROSCOPY (LENS)

The LENS technique relies in the simplest case on the use of a continuous-wave, circularly polarized laser directed into the sample tube of a conventional NMR spectrometer. Following the initial (second-order) theoretical predictions of the present author,[22-30] the first series of LENS experiments[32, 33] has successfully demonstrated the ability of a circularly polarized laser to cause site-specific shifts in NMR resonances. It was found that the shifts were different for each resonating nucleus, for example, ^{1}H and ^{2}D. This means that the technique is capable of providing an entirely new fingerprint of a sample, something that can be interpreted empirically in the analytical, industrial, and biochemical laboratory, in the usual way, without the immediate need for detailed theoretical work of a fundamental nature. For example, the laser-induced shift pattern, as a function of laser intensity and resonance site could lead to an easier interpretation of a very complicated pattern of resonances from identical amino acids in slightly different environments in a protein in solution, a pattern that in the absence of the laser might be indistinguishable, but that in the presence of a laser might become clearly different. This would identify different amino acids residues on the same protein.

The first series of LENS experiments, carried out by Warren and coworkers,[32, 33] set out to detect small shifts caused by a cw argon ion laser of up to 3.0-W/cm^2 intensity, and great care was taken to remove artifacts due to heating. In this section this experiment is described in some detail.

Using data from a series of careful measurements, a small selection of results was presented[32, 33] with 514-nm laser light from a Coherent Innova 200 argon ion laser propagated about 20 m across the laboratory and aimed directly down a 5-mm capillary tube, spinning, as usual in NMR, in a commercial (JEOL GX-270) spectrometer. The laser beam was designed to provide a uniform 10.0-mm diameter at the sample tube, and the wavelength of 514 nm was chosen to be in a transparent part of the sample's visible absorption spectrum (Fig. 3) as a precaution against heating by absorption, and to demonstrate that LENS patterns can be produced with a laser frequency tuned to a transparent[32, 33] as well as an absorbing part of the sample's spectrum.

The results reproduced in Fig. 4 show both bulk and local frequency shifts, and it was found that shifts for a given solute were different in different solvents. Each resonance site has its own shift pattern as a function of laser intensity, which is one example of the new LENS fingerprint. This pattern must, theoretically, be made up of both first-order shift and several types[22-30] of second-order shift, all present simultaneously. In other words, cw laser NMR, even with very low laser intensity, is potentially rich in analytical information. For example, the H resonances of "identical" amino acid residues in different environments of a protein in solution would probably give quite different LENS spectra of the type. Without the need for any further interpretation, it would already have become clear that the two different amino acid residues occupied different sites in the protein, thus the name "laser enhancement."

In future, LENS might well be extended to multidimensional NMR, in which resolution is optimal prior to laser enhancement.[34, 35] In this context, a circularly polarized cw laser provides, in principle, that extra power of analysis that makes the difference between an interpretable LENS fingerprint and an uninterpretable conventional NMR spectrum of heavily overlapping resonance lines in one more dimensions.

Care was taken by Warren and coworkers[32, 33] to minimize heating artifact. This type of artifact is eliminated completely in pulsed-laser NMR (vide infra), being in that case even less of a problem than possible heating caused by the universally employed[34, 35] pulsed radio-frequency field of Fourier transform NMR spectroscopy. In cw laser NMR, however, a laser beam can heat the interior of an NMR tube, a possibility that was countered[32, 33] with specially designed capillary sample tubes, and by gating the laser with a shutter that was controlled by the spectrometer's

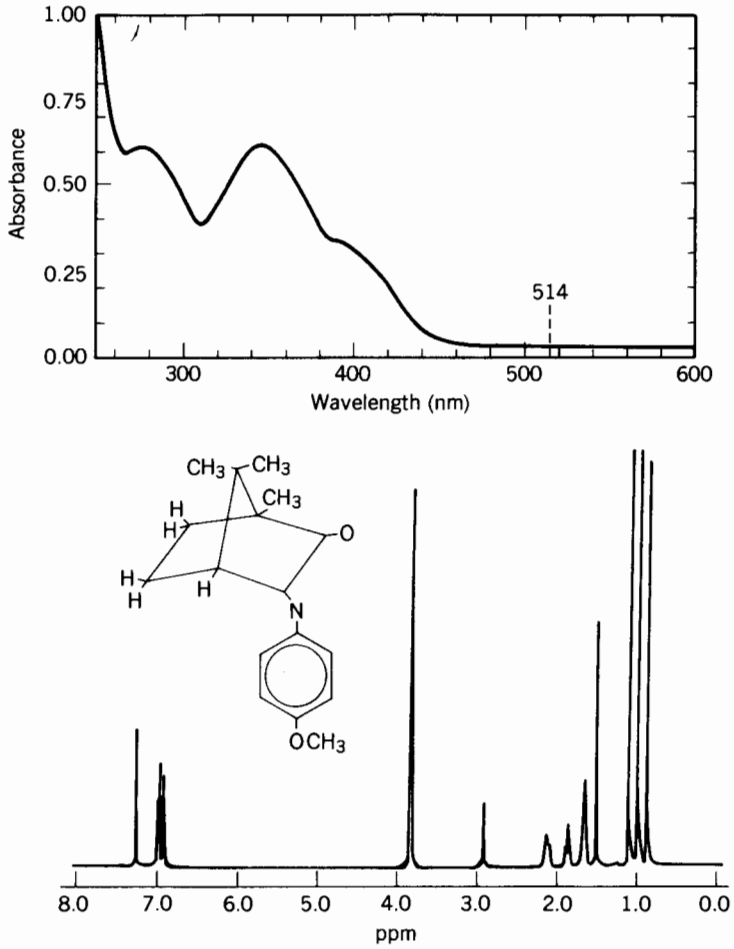

Figure 3. Visible and ultraviolet absorption spectrum (*top*) and 270-MHz NMR spectrum (*bottom*) of *p*-methoxyphenyliminocamphor. (Reproduced by permission from Ref. 33.)

ulse programmer. These measures reduced the power dissipated in the ample itself to at most a few percent of the power delivered by the laser, ar too small to change significantly the temperature of the sample,[33] given ts thermal mass. It was further checked[33] that linearly polarized laser adiation, in which $\mathbf{B}_{\Pi}$ vanishes (Section II), and in which no effect is xpected, produced very small shifts with root mean square uncertainty of nly about -0.15 ± 0.35 Hz (ranging from -0.5 to $+0.2$ Hz, depending n proton site) at the maximum laser intensity used of 3.0 W/cm^2. Note

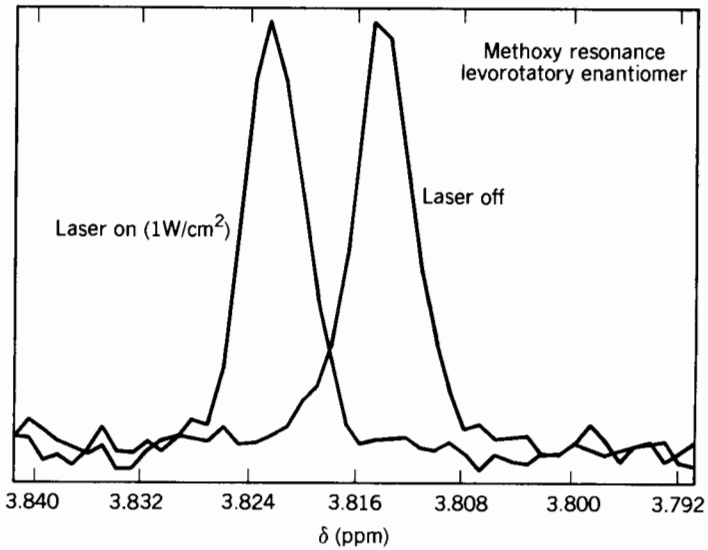

Figure 4. LENS spectrum, showing a typical shift in a resonance line of the sample in Fig. 1 caused by a low-intensity cw circularly polarized laser. (Reproduced by permission from Ref. 33.)

that this compares with a relative laser-induced change in the chemical shift of 2.18 Hz (Fig. 4) generated by a circularly polarized laser in one of the proton resonances and given in terms of 0.008 ppm in Fig. 4. (To convert from ppm to hertz in this context, multiply by the 272-MHz unshielded proton resonance frequency of the JEOL 270 spectrometer, with a magnet of 6.4 T.) Deliberately increasing the sample temperature by 7 K in the absence of any laser radiation was observed[33] to produce a -2.0-Hz shift in the high field ring resonance peaks of the sample, *p*-methoxyphenyliminocamphor, and less than 0.2 Hz, on the average, in the other peaks. The actual temperature increase for maximum laser intensity was estimated to be no more than 3 K, far too low to produce the shift of 2.18 Hz recorded in Fig. 4, which is therefore extremely unlikely to be thermal in origin, and is due to the $\mathbf{B}_{\Pi}$ and $\mathbf{\Pi}^{(A)}$ vectors of a circularly polarized laser. These vectors are responsible, respectively, for first-order[22] and second-order[23–30] resonance shifts in cw (and also pulsed) laser NMR spectroscopy.

The laser-induced bulk shifts were observed by Warren et al.[32, 33] in solvent and solute resonances alike, and it was found that the lock frequency dithered the resonance frequency unless it was blanked when the laser was on. This indicates that the deuterium resonance in deuteri-

ated chloroform is also shifted by the circularly polarized laser. All shifts appeared to go in the direction of increased shielding, independently of the sense of circular polarization. This result probably points toward a dominant first-order mechanism, but much further work is needed to confirm this in other samples and to clarify the role of second-order mechanisms. The observed laser-induced shifts were solvent dependent [33] and were different for the same solute in chloroform and benzene, for example. Local shifts (i.e., shifts in resonances from local protons) were observed which depended on the position of the proton in the molecule and on the handedness of the enantiomer. These important experimental results provide clear first evidence therefore for the theoretical predictions[22-30] that an off-resonance circularly polarized laser can shift (and under certain circumstances split) NMR resonances, and enhance NMR resolution without heating.

The concept of $\mathbf{B}_\Pi$ appears to provide a framework for a simple analysis of these results. The permanent magnetic flux density reported[32, 33] (270 MHz JOEL NMR spectrometer's permanent magnet) is 6.4 T. The extra static magnetic flux density imparted by a circularly polarized laser of 1.0-W/cm^2 intensity is therefore about 2 ppm in absolute terms, about an order of magnitude greater than the relative change, in ppm, in the chemical shift recorded in Fig. 4 in parts per million.[33] In Fig. 4 this is 0.008 ppm for a particular H resonance (methoxy resonance, laevorotatory enantiomer), which converts into 2.18 Hz for the 272-MHz spectrometer used. The experimental data are consistent in the first approximation with an interaction energy of the form

$$E_3 = -\mathbf{m}^{(N)} \cdot [\mathbf{B}_0(1 - \sigma_1) \pm \mathbf{B}_\Pi(1 - \sigma_2)] \tag{42}$$

where σ_2 is the chemical shift constant in the presence of the laser for a particular resonating nucleus. The shielding constant σ_2 appears to be different in general from its equivalent without the laser because the latter can also generate an extra magnetic field at the nucleus due to Fermi contact interaction[23] and other second-order effects.[24-30] Without these second-order mechanisms there is no reason why the constant σ_1 should change, but the absolute value of the chemical shift in hertz is increased because the effective external magnetic field is increased from $\mathbf{B}_0$ to $\mathbf{B}_0 + \mathbf{B}_\Pi$ by the laser. Therefore, the laser increases the spectrometer's effective resolution and gives a new pattern of chemical shifts.

On the basis of Eq. (42) the simplest type of interaction energy is an absolute proton resonance shift of 425.78 Hz, equivalent to a $\mathbf{B}_\Pi$ of 10^{-5} T. (Note that the shift in Fig. 4 is expressed in parts per million, and is a unitless ratio[34] of resonance frequencies, not an absolute laser-induced shift expressed in hertz.) On this same scale, a permanent NMR magnet of flux density of 6.4 T is equivalent to 272.5 MHz. Therefore, it is expected that the absolute value in hertz of the chemical shift, originally $\delta_1 B_0$, is changed by the laser to $\delta_2 B_0$. On the basis of the first-order interaction (42), parameter δ_1 itself, for a given resonance site, should not change to first order, but to second order such a change is expected due to Fermi contact[23] and other mechanisms. The result reproduced in Fig. 4 indicates that the expected absolute, laser-induced frequency shift for the unshielded proton resonance (425.78 Hz for a $\mathbf{B}_\Pi$ of 10^{-5} T), is different for different proton sites. In the case of the methoxy proton in Fig. 4, the laser-induced shift relative to the standard resonance frequency is changed by 2.18 Hz from the equivalent in the absence of the laser. This is the type of change that forms the useful site-selective, laser-induced, resonance fingerprint.

Theoretically, a very intense laser pulse is capable of increasing dramatically the absolute frequency separation of the original NMR resonances, and therefore capable of increasing the effective resolution of the conventional NMR spectrum of any type (one or n dimensional). If this were realized in practice it might be a useful development in several types of NMR spectroscopy.

In summary, a laser of $\mathbf{B}_\Pi = 10^{-5}$ T is expected to produce an unscreened proton shift of 425.78 Hz in the first-order mechanism.[22] In addition, there are other, second-order, mechanisms that are expected to produce smaller shifts, as described in the literature. Among these are shifts due to the vectorial polarizability,[24] hyperpolarizability shifts,[25, 26] and shifts due to Fermi contact interactions.[23] The various types of shift are not mutually independent, but result in angular momentum coupling, illustrated briefly in the following example for atoms with net electronic spin such as H and various metal atoms in the ground state.[27]

A. Angular Momentum Coupling: Atomic Model

We have seen that a circularly polarized laser generates the magnetic flux density $\mathbf{B}_\Pi$ in its axis of propagation, and that the pure imaginary conjugate product $\mathbf{\Pi}^{(A)}$ is built up from the pure real $\mathbf{B}_\Pi$ by multiplication by i and a T- and P-positive scalar constant. The real, static, flux density appears to be a novel fundamental property of circularly polarized electromagnetic radiation (of any frequency), and forms an interaction energy with any type of magnetic dipole moment, and in LENS the latter is a nuclear magnetic dipole moment $\mathbf{m}^{(N)}$. However, the conjugate product $\mathbf{\Pi}^{(A)}$ is also capable of forming a scalar interaction energy (Appendix B):

$$E_4 = i\boldsymbol{\alpha}'' \cdot \mathbf{\Pi}^{(A)} \tag{43}$$

where $i\boldsymbol{\alpha}''$ is the imaginary part of the atom's or molecule's electronic electric polarizability. Clearly, $\boldsymbol{\alpha}''$ must be T negative and P positive, and also an axial vector if this energy is to be a T- and P-positive scalar. The required vectorial form is obtained[36, 37] from the usual tensor α''_{ij} by tensor multiplication with the rank three, totally antisymmetric unit tensor, known as the Levi-Civita symbol[36, 37]:

$$\alpha''_k = \varepsilon_{ijk}\alpha''_{ij} \tag{44}$$

Neglecting the chemical shift screening constants in the first approximation, the complete (first- plus second-order) interaction Hamiltonian is therefore

$$E_5 = -\mathbf{m}^{(N)} \cdot (\mathbf{B}_\Pi + \mathbf{B}_0) + i\boldsymbol{\alpha}'' \cdot \boldsymbol{\Pi}^{(A)} \tag{45}$$

and in general there is angular momentum coupling (for example, Landé coupling[31]) between the two terms. This is a quantum-mechanical phenomenon, which further enriches the LENS spectrum in theory. It is akin to the family of angular momentum coupling phenomena such as spin–orbit and coupling and spin–rotation coupling, measurable in such phenomena as the anomalous Zeeman effect.[31] The fundamental reason for the phenomenon in the context of the energy (45) is that the vectors $\mathbf{m}^{(N)}$ and $\boldsymbol{\alpha}''$ are both proportional to a quantized angular momentum, and these two angular momenta do not commute in general, in the same way that orbital and spin electronic angular momentum vectors do not commute in the anomalous Zeeman effect Hamiltonian.[31] It is revealing to write the vectorial polarizability in terms of an induced electronic magnetic dipole moment:

$$\mathbf{m}^{(\text{ind})} = 2c^2 B_0 \boldsymbol{\alpha}'' \tag{46}$$

showing clearly that $\mathbf{m}^{(\text{ind})}$ and $\boldsymbol{\alpha}''$ have the same fundamental symmetries, i.e., T-negative, P-positive axial vector symmetry. Being an electronic magnetic dipole moment, $\mathbf{m}^{(\text{ind})}$ can be written as

$$\mathbf{m}^{(\text{ind})} = 2c^2 B_0 \gamma_\Pi \mathbf{J} \tag{47}$$

where $\mathbf{J}$ is the electronic angular momentum and γ_Π the gyroptic ratio.[24] The interaction energy[45] therefore becomes

$$E_5 = -\gamma_N \mathbf{I} \cdot (\mathbf{B}_\Pi + \mathbf{B}_0) - 2c^2 B_0 \gamma_\Pi i(\mathbf{L} + 2.002\mathbf{S}) \cdot \mathbf{B}_\Pi \tag{48}$$

implying that the laser-induced electronic magnetic dipole moment is proportional to the sum $\mathbf{L} + 2.002\mathbf{S}$ of orbital and spin electronic angular momenta components in the laser's propagation axis. The interaction energy (48) therefore consists in general of three noncommuting angular momenta.[29, 30] For atoms, these are $\mathbf{I}$, the nuclear spin angular momentum, $\mathbf{L}$, the electronic orbital angular momentum, and $2.002\mathbf{S}$, the electronic spin angular momentum. The electronic spin angular momentum is the only contribution to the vectorial polarizability[29, 30] in the $J = \frac{1}{2}$ ground state of an atom, for example, and for this reason the electron has spin polarizability,[38] a property that has been computed ab initio in some cases by Manakov et al.[8–10] To understand this property, recall that electronic spin is a relativistic quantity in theory, and the term does not imply a physically spinning object. A fuller understanding of spin polarizability must therefore be sought in the Dirac equation, taking into account such effects as Thomas precession.[31]

Using the standard methods of quantum mechanics, the interaction energy can be developed in terms of coupled eigenstates, as usual:

$$\begin{aligned} E_5 = &-\langle LSJIFM_F|\gamma_N I_Z(B_{\Pi Z} + B_{0Z}) \\ &+ 2B_0 c^2 \gamma_\Pi (L_Z + 2.002S_Z) B_{\Pi Z}|L'S'J'I'F'M'_F\rangle \end{aligned} \tag{49}$$

in the coupling scheme

$$\mathbf{J} = \mathbf{L} + \mathbf{S} \qquad \mathbf{F} = \mathbf{J} + \mathbf{I} \tag{50}$$

from which the LENS resonance frequency can be calculated[30] to be

$$\hbar\omega_R = \frac{|2B_0 c^2 \gamma_\Pi B_{\Pi Z}(g_1 + 2.002g_2) + g_N \gamma_N (B_{0Z} + B_{\Pi Z}) g_3|}{[F(F+1)(2F+1)]^{1/2}} \tag{51}$$

where the g factors are evaluated with the usual 9-j symbols. For reasonable values of the quantum numbers L, S, and I in atoms with net electronic spin, we obtain results that show that the c.p. laser causes a shift to higher resonance frequencies, a shift that is linear in the square root of the intensity to first order, and linear in the intensity to second order. The combined effect of the laser's properties $\mathbf{B}_\Pi$ and $\boldsymbol{\Pi}^{(A)}$ is to enrich greatly the original resonance spectrum.

B. Interrelation of Some Molecular Property Tensors

In Section III.A, an example was given of a novel interrelation between molecular property tensors, Eq. (46), which shows that the antisymmetric

(or vectorial) polarizability is directly proportional to an induced electronic magnetic dipole moment $\mathbf{m}^{(\mathrm{ind})}$. It follows that the irreducible representations of these vectors are the same in all molecular and atomic point groups, and in the group of all rotations and reflections[39] of an ensemble in the laboratory frame. Furthermore, it is reasonable to conclude that a permanent magnetic dipole moment (nuclear or electronic), must also transform as a higher rank molecular property tensor of some kind, because any axial vector (i.e., rank one tensor) is simultaneously definable as a second rank, antisymmetric, polar tensor.[36] In the case of a nuclear magnetic dipole, this conforms with the fact that a nucleus has an electric polarizability, whose antisymmetric component is proportional to its magnetic dipole moment, which can occur in both protons and neutrons.[31]

Whenever a magnetic dipole moment occurs in a given spectroscopic situation it must have the same fundamental symmetries as vectorial electric polarizability, and the same is true of the corresponding quantum-mechanical operators. On the grounds of symmetry and tensor algebra, such interrelations can also be constructed between other ranks of tensors, such as rank three hyperpolarizabilities of various kinds, by replacing the magnetic dipole moment wherever it occurs by the vectorial electric polarizability. These relations provide insight to the fundamental nature of both the magnetic dipole moment and the antisymmetric electric polarizability.

A relation can also be forged between the vectorial polarizability and the magnetizability by considering the sample in the simultaneous presence of both a circularly polarized laser and permanent magnetic flux density. In this case the interaction energy between the laser-induced magnetic dipole moment and the magnetic flux density of the permanent magnet can be written in the simplest case as (see also Appendix B)

$$E_6 = -\mathbf{m}^{(\mathrm{ind})} \cdot \mathbf{B}_0 = -2c^2 B_0 \alpha''_Z B_{0Z} \tag{52}$$

Comparing this expression with Eq. (14.2.9) of Atkins[31] yields a relation between the vectorial polarizability and the magnetizability

$$\xi_Z^{(\Pi)} = 2c^2 \mu_0 \alpha''_Z \tag{53}$$

which can be written equivalently as

$$\xi_{XY}^{(\Pi)} = -\xi_{YX}^{(\Pi)} = 2c^2 \mu_0 \alpha''_{XY} \tag{54}$$

where $\xi_{XY}^{(\Pi)}$ is the laser-induced magnetizability of the sample in the presence of a static magnetic field. We have therefore forged relations between the magnetic electronic dipole moment, the vectorial electric electronic polarizability, and the magnetizability.

IV. PULSED-LASER NMR AND ESR SPECTROSCOPY

The LENS method as developed to date uses a low-intensity cw laser in the sample tube of an NMR spectrometer. By looking at Eq. (23) it can be seen that a pulsed laser delivering a nonzero $\partial \mathbf{B}_\Pi / \partial t$ over an interval t also generates an electric field $\mathbf{E}_\Pi$ whose curl is no longer zero. This electric field can be picked up as a signal and stored in the computer of a contemporary Fourier transform NMR spectrometer. It is well known that laser pulses can be very short and intense. For example,[40] a passively mode-locked dye laser give 0.5 GW of power in about 0.4 ps at a frequency of about 600 THz in the visible. For a laser aperture of 1.0 cm^2 this gives an intensity I_0 of 5.0 TW/m^2. If focused to 1.0 mm^2 the intensity is increased 100 times. In contrast, a continuous-wave argon ion laser such as the one used in the first LENS demonstration[33] provides an intensity twelve orders of magnitude lower, up to about 3.0 W/cm^2, but still results in easily measurable and very useful NMR shifts. We have seen that first-order shifts due to $\mathbf{B}_\Pi$ are proportional to the square root of the laser's intensity, and second-order shifts are proportional to the intensity itself. In principle, therefore, very large shifts to higher frequency (enormous increases in effective resolution) are possible using a circularly polarized laser. There appear to be several other ways, however, of incorporating a laser pulse in NMR spectroscopy, relying specifically on the use of the Fourier transform,[34, 35, 41] which appear to be technically less of a challenge, and which are introduced as follows.

Contemporary Fourier transform NMR and ESR technology is mature and highly diversified after 50 years of development. Consequently, it is of advantage to incorporate a laser pulse as directly as possible into the contemporary designs,[35, 41] and it is shown in this section that the 180° radio-frequency pulse generated in a conventional spectrometer can be augmented by a pulse of magnetization from a circularly polarized laser radiation.

It is well known[35, 41] that the essence of Fourier transform NMR spectroscopy is the measurement of free induction decay following radio-frequency pulses and pulse sequences. In the simplest case a sample is excited with a 90° pulse, and the free induction decay is Fourier transformed, as first demonstrated by Ernst and Anderson.[42] The magnetization pulse is achieved with a rotating and linearly polarized radio-frequency field at right angles to the static magnetic field of the bit NMR magnet. One of the circularly polarized components of the rf field rotates in the

same sense as the nuclear spins. The so-called 90° pulse rotates the spins perpendicular to the $\mathbf{B}_0$ of the big magnet, and causes nonzero, mean transverse magnetization. After the pulse has passed through the sample, the transverse magnetization ($\mathbf{m}_t$) returns to the original equilibrium state in the presence of $\mathbf{B}_0$, an equilibrium in which $\mathbf{m}_t$ is zero on average. This forms the free induction decay signal, which is stored in a computer and whose Fourier transform is a high-resolution NMR spectrum. There are many important and widely used variations on this theme such as two- and multi-dimensional NMR and Fourier transform NMR imaging. The rf pulse simulates an impulse function, which, ideally, is a delta function in time. However, a single rf pulse is microseconds in duration in practice, so that its Fourier transform is a complicated oscillatory function of frequency, usually of the type $(\sin x)/x$. The technique is practical because the characteristic relaxation times of nuclear spin relaxation are much longer than the rf pulse, but nevertheless, the free induction decay is the required (true) impulse response function only when the impulse itself is a true delta function in time.

Another widely used rf pulse is the Π (180°) pulse, which reverses the net longitudinal magnetization of the sample without generating nonzero mean transverse magnetization. A pulse of $\mathbf{B}_\Pi$ from a circularly polarized laser has the same characteristics, and therefore can be used in a contemporary NMR spectrometer in exactly the same way as a radio-frequency Π pulse.

Consider an ensemble of spin-$\frac{1}{2}$ nuclei at equilibrium in the presence of the ultrahomogeneous magnetic field of a big NMR magnet, such as a 6.4-T superconducting magnet of a JEOL 270 spectrometer. There are two different energy levels, corresponding to $M_I = +\frac{1}{2}$ and $M_I = -\frac{1}{2}$. According to Boltzmann statistics, there is a slight excess of spins in the lower energy level when the two are in thermodynamic equilibrium, a condition in which there is net longitudinal magnetization in the Z axis of the magnetic field, but no transverse magnetization. Each nuclear magnetic dipole moment precesses around a cone of half-angle θ at a classical angular velocity $\gamma_N B_0$, where γ_N is the nuclear gyromagnetic ratio. In a time t the motion covers an angle of $\gamma_N B_0 t$ in radians (one radian is about 57°). There is no observable resonance signal in this equilibrium condition; such a signal requires a synchronization of spins, achieved with the rotating magnetic field of the rf coil described already as the mechanism responsible for the $\pi/2$ (90°) pulse.

The net nuclear magnetization in this condition is the sum, or number density, of nuclear magnetic dipole moment vectors:

$$\mathbf{M} = N_0\langle \mathbf{m}^{(N)} \rangle \tag{55}$$

where $\langle \mathbf{m}^{(N)} \rangle$ is the mean value of the magnetic dipole moments and N_0 the number density. The interaction energy of $\mathbf{B}_0$ and $\mathbf{m}^{(N)}$ is $-\mathbf{m}^{(N)} \cdot \mathbf{B}_0$ and the Boltzmann weighted average of $m_Z^{(N)}$ at a temperature T is

$$\langle m_Z^{(N)} \rangle = m_Z^{(N)} \mathscr{L}(x) \qquad x = \frac{m_Z^{(N)} B_{0Z}}{kT}; \tag{56}$$

where $\mathscr{L}$ is the well-known Langevin function. The magnetization in the Z direction is therefore

$$M_Z \doteq \frac{N_0 m_Z^{(N)^2} B_{0Z}}{3kT} \tag{57}$$

which is proportional to the applied static magnetic field and is in the direction of $\mathbf{B}_0$. So if we reverse $\mathbf{B}_0$ we must reverse $\mathbf{M}$. The Langevin function is calculated[31] from the average nuclear dipole moment density $N_0 m_Z^{(N)} \mathscr{L}(x)$ and from the fact that at a temperature T the proportion of molecules with orientation θ in the range θ to $\theta + d\theta$ is the Boltzmann distribution

$$\frac{dN_0(\theta)}{N_0} = \frac{\exp\left(m_Z^{(N)} B_{0Z} \cos\theta/kT\right)\sin\theta\, d\theta}{\int_0^\Pi \exp\left(m_Z^{(N)} B_{0Z} \cos\theta/kT\right)\sin\theta\, d\theta}. \tag{58}$$

This number depends on the magnitude and direction of $\mathbf{B}$. The Langevin function has an initial value of zero and rises to a saturation value of unity:

$$\mathscr{L}(x) = \frac{e^x + e^{-x}}{e^x - e^{-x}} - \frac{1}{x} \tag{59}$$

Classically, therefore, the longitudinal magnetization $\mathbf{M}$ is proportional to the thermodynamic average of the quantity $\cos\theta$. Clearly, if θ approaches zero, $\mathbf{M}$ approaches its maximum, and as θ approaches 90°, $\mathbf{M}$ approaches a minimum. If θ approaches 180° the sign of $\mathbf{M}$ is reversed, and, conversely, if the sign of $\mathbf{M}$ is reversed, θ is changed by 180°. This last property is critical to the use of a pulsed laser to create a 180° pulse. A pulse of magnetization created by $\mathbf{B}_\Pi$ applied in the Z axis changes or "flips" the angle θ, and the extent of the change depends on the time for which the pulse is applied. In this process the half-angle of the cone defining the precession changes, but the axis of the cone remains on average the Z axis of the magnetic field, because no transverse magnetization is created by the laser pulse.

A pulse if circularly polarized laser radiation traveling in Z through a sample tube of a contemporary Fourier transform spectrometer, parallel or antiparallel with $\mathbf{B}_0$ of the big magnet, will cause $\mathbf{B}_0$ to change to $\mathbf{B}_0 \pm \mathbf{B}_\Pi$, depending on the direction of travel of the laser and its circular polarization (right or left). The more intense the laser, the greater is $\mathbf{B}_\Pi$ (Eq. (14)). In this situation the Larmor precession frequency changes to

$$\omega_1 = \gamma_1 B_{0Z} \tag{60}$$

where

$$\gamma_1 = \gamma_N \left(1 \pm \frac{B_{\Pi Z}}{B_{0Z}} \right) \tag{61}$$

is the new effective gyromagnetic ratio (nuclear (NMR), or electronic (ESR)). If a pulse of circularly polarized laser radiation passes through the sample, its pulse frequency is

$$\mathrm{f} = \frac{\gamma_N B_{\Pi Z}}{2\pi} \text{ hertz} \tag{62}$$

and the angle θ is defined by

$$\theta = \gamma_N B_{\Pi Z} t \tag{63}$$

in radians, where t is the pulse duration in seconds.

If $\mathbf{B}_\Pi$ suddenly increases $\mathbf{B}_0$ of the permanent magnet of the instrument, the extra $\mathbf{B}_\Pi$ will change the minimum energy alignment in the field $\mathbf{B}_0$, but will not create mean transverse magnetization, as we have argued. This is precisely what happens with the conventional 180° rf pulse. We conclude that a laser can act in contemporary NMR spectrometers in exact analogy with the widely used 180° rf pulse, leading in principle to numerous technological possibilities provided that there is simultaneous synchronization of spins. If $I = \frac{1}{2}$, for example, there are two nuclear spin states, as usual. If $\mathbf{B}_0$ is suddenly increased to $\mathbf{B}_0 \pm \mathbf{B}_\Pi$ by the laser pulse, the energy separation between the two spin states is increased, and therefore the number of spins is expected to remain in the lower energy state,[34] i.e., the new equilibrium value of longitudinal magnetization $\mathbf{M}$ is increased. The system will respond to the laser pulse by means of spins undergoing transitions from the upper to lower energy levels, defined by

the laser-on Boltzmann distribution

$$\frac{N_{\text{higher}}}{N_{\text{lower}}} = \exp\left[- \frac{2\mathbf{m}^{(N)} \cdot (\mathbf{B}_0 + \mathbf{B}_\Pi)}{kT} \right] \tag{64}$$

where N_{higher} and N_{lower} are the numbers of higher and lower energy state spins, respectively, and $\mathbf{m}^{(N)}$ is the permanent nuclear magnetic dipole moment. This process involves a loss of energy by the system over time T_1, the longitudinal spin–lattice relaxation time. It is well known[34] that T_1 can be as long as 1000 s, many orders of magnitude longer than a typical high energy laser pulse (vide infra). Conversely, if $\mathbf{B}_\Pi$ opposes $\mathbf{B}_0$, spins will go from lower to upper energy levels, a process involving a gain of energy over a time T_1.

In a laser-generated 180° pulse, therefore, there is no mean transverse magnetization, and the lower energy spins are converted to higher energy ones by a laser producing $-\mathbf{B}_\Pi$. After the laser pulse passes through the spinning sample tube of the NMR spectrometer, the spins relax to their normal state in $\mathbf{B}_0$ of the permanent magnet with a characteristic longitudinal relaxation time T_1. This process in itself produces no resonance effects and no signal, as with a conventional 180° pulse.[34] However, the resonance effect of the laser pulse can then be detected a time $t = \tau$ after the pulse by the application of a conventional 90° radio-frequency pulse. A simple pulsed NMR sequence is therefore

$$180° \text{ laser pulse} - \tau - 90° \text{ radio-frequency pulse} \tag{65}$$

A. Numerical Estimates

Consider a pulse of circularly polarized giant ruby laser radiation, with an intensity of 10^{11} W/m^2 and a pulse duration of 30 ns (Refs. 1–4). These were the characteristics used[1–4] to demonstrate the inverse Faraday effect. The laser generates a $\mathbf{B}_\Pi$ of about 0.03 T from Eq. (14) over 30 ns, which rotates the spin by an angle of about 0.1 radians (about 6°) from Eq. (63). This is increased to about 60° by focusing the laser to an intensity 100 times greater. Following the passage of the pulse through the sample, there is a laser-induced longitudinal relaxation, followed τ seconds later by the 90° measuring radio-frequency pulse tuned as usual to resonance.

Clearly, any flip angle θ can be generated by adjusting the duration and/or intensity of the circularly polarized laser pulse. The terminology "180° laser pulse" should therefore not be taken to imply that the angle θ must be exactly 180°, because free induction decay will always occur if the spins are tilted out of their initial equilibrium in the big magnet's static

field. There is no difficulty in principle in extending the method for use in a contemporary pulse sequence, and this is developed below for spin-echo, two-dimensional, and other types of pulsed Fourier transform laser NMR. For example, laser spin-echo resonance can be achieved by generating a 90° rf pulse, followed a time τ later by a 180° laser pulse to reverse and refocus the spins, so that τ seconds after the laser pulse the spins all precess back into phase, producing the "laser echo."

It is a great advantage to time the laser pulse to be of exactly the same duration as a conventional 180° radio-frequency pulse applied simultaneously. This would have the advantages of synchronizing the spins and of effectively increasing the field from $\mathbf{B}_0$ to $\mathbf{B}_0 + \mathbf{B}_\Pi$ at exactly the same time, resulting in greatly increased instrumental resolution. In what follows, this is the 180° laser pulse.

B. Some Advantages of the Laser Pulse

A 180° laser pulse can be designed to be as much as ten million times shorter in duration than its radio-frequency relative, so that the laser pulse is a far better approximation to a perfect impulse function (a delta function of infinitely short duration and infinite intensity). This implies that the bandwidth, $1/t$ hertz, associated with the laser pulse is up to ten million times greater, and that the Fourier transform of the impulse function due to the laser pulse is almost a perfect impulse response function, a constant in frequency.[35] In principle, therefore, the laser produces much less of a problem in deconvoluting the free induction decay. Many different laser systems are available that can give a large variety of pulse lengths and intensities. Another potential advantage of laser pulses is that they can be designed to occur on the picosecond time scale[43] of molecular motion and interaction, and chemical reactions in the liquid state.[44] Therefore, pulsed-laser NMR can be used in principle to study molecular dynamics and reaction processes in solution, and with technical ingenuity,[41] laser imaging NMR is a possibility (vide infra). Laser pulses can be designed to be hard pulses (square wave), or to have a Gaussian profile,[44] for example, and in general the 180° laser pulse generates uniform excitation[35] over a very much greater range of frequencies than its rf equivalent. The flip angle θ generated by the laser pulse is determined by Eq. (63) and depends on the product of $\mathbf{B}_{\Pi Z}$ and t for a given nuclear gyromagnetic ratio. The ideal delta impulse function is approached, furthermore, with an ultra short, ultra intense 180° laser pulse, using contemporary mode-locking technology with, for example, dye lasers.[45]

The flip angle need not be exactly 180°, provided that the 180° laser pulse is followed by the free induction decay of the laser flipped spins, a

decay that is governed by the longitudinal spin–lattice relaxation time T_1 and that is picked up and analyzed by the recovery pulse,[35] a conventional 90° rf pulse. We call this method the laser inversion—recovery (LASEI) sequence. It is one of several ways in which pulsed laser Fourier transform NMR can be developed in principle. Other methods are reviewed later. The LASEI method is easy to use by incorporating a 180° laser pulse in the right place and at the right time in an otherwise conventional NMR spectrometer. The response of the nuclear spins to the laser pulse is measured through a suitable free induction decay, i.e., the induction of electromotive force in the receiver coils of the spectrometer,[35] a signal that is stored in the computer memory as usual. The conventional 90° rf pulse is used as usual in an inverse–recovery experiment, to measure the extent to which the longitudinal magnetization caused by $\mathbf{B}_\Pi$ has decayed with a characteristic longitudinal relaxation time T_1. (Conventionally, the longitudinal relaxation is that of magnetization due to a 180° rf pulse.)

This method can be applied to liquids, solids, and gases, or any material with a suitable nuclear magnetic dipole moment, and is in principle full of potentially new information because the laser pulse generates a variety of novel second-order effects[23–30] as well as the first-order magnetization due to the interaction energy of $\mathbf{m}^{(N)}$ and $\mathbf{B}_\Pi$. The second-order effects cause Landé coupling[30] which can in theory split as well as shift existing NMR resonances and whose selection rules are also different from those of conventional NMR.[31] These effects are all present in the laser-induced free induction decay following the 180° laser pulse, and by Fourier transformation give a spectrum of resonances that can be picked up with the measuring 90° rf pulse of the spectrometer.

The above depends on the assumption that if $\mathbf{B}_0$ is suddenly changed to $\mathbf{B}_0 \pm \mathbf{B}_\Pi$ by a laser pulse in the Z axis, there is no net (average) transverse magnetization generated, but that there is an increase in energy separation between the two nuclear spin state of, for example, an H nucleus, so that the new equilibrium value of longitudinal magnetization is increased and the original precession cone axis[35] is not tipped by transverse magnetization. (The cone's mean radius changes with the flip angle θ; If this is 180°, then the cone is pulled inside out by the laser pulse, but the cone's axis is still aligned on average in Z, the direction of the permanent magnet's field.)

The 180° laser pulse has several advantages and has the effect of changing the delicate equilibrium between spins and external permanent magnetic field in a conventional NMR spectrometer, introducing net longitudinal magnetization, which disappears as free induction decay after the pulse has passed through the sample. The Fourier transform of this free induction decay contains information on the way in which the laser

imparts magnetization to the ensemble of nuclear spins, information that can be used to analyze in a new way the nature of the sample under investigation.

C. Application to Molecular Dynamics and Chemical Reactions, or Similar Dynamical Processes

It it well known that a laser pulse on the femtosecond or picosecond scale acts as camera shutter on molecular dynamical processes[44] taking place on a similar time scale, and effectively freezes them for measurement. In the particular context of pulsed-laser NMR, the duration and intensity of the circularly polarized laser pulse determines the flip angle and the extent of magnetization produced prior to free induction decay. The nature of the free induction decay following the pulse is therefore determined by the dynamics of the molecules in which the nuclear spins are situated. The laser pulse does not cause the nuclear magnetization to rise immediately (in an infinitely short time) from zero to a final level, but initiates a rise transient of nuclear spins, a process that occupies a finite interval of time, presumably on the femtosecond scale. Nothing appears to be known about the nuclear spin rise transient, which can be investigated in principle by varying the length and intensity of the laser pulse and measuring the resulting free induction decay with a 90° rf pulse to produce the resonance spectrum.

Molecular dynamical rise transients are well known in several different contexts and can be simulated by computer,[46] for example. Similarly, the degree of magnetization for a given pulse depends on the $\mathbf{B}_\Pi$ field of the laser to first order, an don its $\mathbf{\Pi}^{(A)}$ vector to second order, and the final level attained by the transient is governed by a Langevin or Langevin–Kielich function.[47] In much the same way as the T_1 decay time is affected by Brownian motion (more accurately, molecular dynamics[43]) so is the T_1 rise time in response to a laser pulse. This aspect appears not to be considered in conventional Fourier transform NMR spectroscopy, so that it is apparently assumed that the rise transient of nuclear magnetization must be effectively very short on the microsecond scale of the conventional radio-frequency pulse. This is no longer tenable if the nuclear spin–rise transient and the laser pulse both occur on the same time scale, as seems inevitable when the laser pulse is only femtoseconds in duration.

In this eventuality the degree of longitudinal magnetization is presumably proportional to the saturation level of the nuclear spin–rise transient, a level that in a molecular context is well known[46, 47] to depend on the nature of the dynamics (saturation values of rise transients form Langevin or Langevin–Kielich functions). Conversely therefore, the degree of magnetization following a laser pulse provides valuable information in principle on the molecular dynamical processes affecting nuclear magnetization, processes that occur on the picosecond or femtosecond scale in gases and liquids, for example. Again, a chemical reaction taking place on this time scale can be monitored by using a series of LASEI measurements, varying the laser pulse duration. The result is a series of longitudinal free induction decay curves that can be picked up for analysis by the 90° rf pulse and interpreted to give information on the progress of the reaction on the femtosecond time scale.

D. Laser Spin-Echo NMR Spectroscopy

In this type of pulsed laser NMR spectroscopy the 180° laser pulse would be used to refocus phase coherence.[35] To modify the conventional and well-known Carr–Purcell sequence for use with a pulsed circularly polarized laser, transverse magnetization would first be created with a conventional rf 90° pulse magnetization, which is allowed to decay over an interval of time τ, during which the phase coherence of individual spin vectors is being lost.[35] A 180° laser pulse is then applied in the $+Y$ axis (perpendicular to the Z axis of the big magnet's field) to recreate the phase coherence, which is detected as a laser-induced spin echo. This method would implicitly have all the advantages of the laser 180° pulse discussed already, for example, an effectively infinite bandwidth in hertz.

E. Selective Population Transfer with a Laser Pulse

When a selective 180° laser pulse is applied to an I spin transition,[35] the spin populations are changed, resulting in a change in the intensities of S spin transition resonance lines of a weakly coupled two-spin $\frac{1}{2}$ system IS.[35] This is a laser-induced selective population transfer, a phenomenon that can be used to demonstrate the magnetization effect of a laser pulse in, for example, a system with a proton attached directly to a resonating ^{13}C nucleus. The selective population transfer experiment has been replaced in conventional technology by two-dimensional NMR methods, but appears to be useful in the above context.

F. Solid-State Laser NMR Spectroscopy

In conventional solid-state NMR spectroscopy, resonances are very broad and conventional methods such as magic angle spinning[35] are used in an attempt to narrow them and to resolve the underlying resonance spectrum. Efficient narrowing of solid-state NMR spectra would open up many new areas of investigation in the condensed state of matter. A conventional method that could be adopted for use with lasers in principle is pulse

spinning,[35] where magnetic spin–spin interactions (the source of broadening) are averaged out by forcing the spins in the solid lattice to change quickly and selectively about a magnetic field direction by applying 90° rf pulses along both the X and Y axes and alternating their phases.[35] Conventionally, this requires "short" (microsecond) and intense rf pulses, and the technology needed for this is difficult to implement, requiring rf pulse trains of up to about 52 individual pulses. The data are sampled during intervals in the pulse train[35] and stored in a computer. The essence of the method is that individual chemical-shift directional anisotropies in, for example, a crystal are determined by both the parallel and perpendicular magnetic field components during a pulse train.

In principle, it appears much easier to implement a train of suitably aimed 180° laser pulses to "scramble" the nuclear spins and average out the spin–spin coupling and magnetic anisotropies that cause solid-state NMR broadening. Laser pulses are much more intense and of much shorter duration than rf pulses, and contemporary laser pulse train technology is highly developed. The effect of the laser pulses could be picked up using a suitable LASEI sequence, for example, and the technique, if developed, appears to have considerable merits.

V. LASER-IMAGING NMR SPECTROSCOPY

The key to laser-imaging NMR spectroscopy is to introduce deliberate inhomogeneities into the $\mathbf{B}_0$ of the big permanent magnet by scanning the sample (for example, a tissue mounted on a slide) with a circularly polarized laser, so that at each spot the effective field is increased to $\mathbf{B}_0 \pm \mathbf{B}_\Pi$ from $\mathbf{B}_0$, introducing an effective change

$$\delta \mathrm{f} = \pm \frac{\gamma_N \mathbf{B}_{\Pi Z}}{2\pi} \text{ hertz} \tag{66}$$

in the resonance frequency at that spot. In principle, spatial information about the sample (an image) becomes available through the laser-induced shift in the effective applied magnetic field at that spot. This is similar to conventional NMR imaging, where the frequency shift is introduced with deliberately imposed magnetic field gradients, but the image in laser NMR is built up with a different scanning principle. As the laser passes across a given spot, the field $\mathbf{B}_0 \pm \mathbf{B}_\Pi$ induces a resonance whose intensity at that spot is proportional to the number of equivalent spins per unit volume contained there. The resonance signal recorded by the instrument is therefore proportional to the density of spins at that spot, which is recorded in a computer equipped with state of the art imaging software.

Using well-developed laser scanning technology, a sample can be scanned many thousands of times if needs be, and the average image built up in two dimensions. A three-dimensional image is constructed as in conventional[4] projection–reconstruction imaging NMR by rotating the sample.

It appears at this stage that the image might well be optimized in quality by making use of Fourier transform imaging techniques[41] with the incorporation of laser pulses. Each spot in the sample could be examined in this way with optimization of image quality using a LASEI sequence for each spot. The free induction decay following the 180° laser pulse at that spot would be unique, and an image could be computed from a knowledge of the details of the LASEI spectrum at each locality in the specimen. It appears possible to use trains of scanning laser pulses, whose average effect would be recorded at any given spot in the sample, data reduction being a matter of software ingenuity. Laser echo line imaging is another possibility,[4] the key idea of which would be to use a 180° selective laser pulse in the presence of a conventional 90° rf detection/resonance pulse in the presence of a conventional g gradient.[4] This pulse rotates the spins of a selected plane perpendicular to the Z axis, and the difference between two induction signals, one with and one without the 180° laser pulse, is used to give the required signal. In this method, the 180° laser pulse has all the advantages of being an effectively perfect impulse function.

VI. MULTIDIMENSIONAL LASER NMR SPECTROSCOPY

The incorporation of 180° laser pulses into the highly developed contemporary technology in this field relies again on the replacement of the 180° rf pulse. In one-dimensional Fourier transform NMR[35] the free induction decay is a function of a single time variable,[35] which is supplemented in two-dimensional NMR by the introduction of a second time variable τ_2. A series of free induction decay curves is collected as a function of τ_2 and double Fourier transformation[35] gives a spectrum that is a function of two frequency axes, with many advantages. An example of how a laser pulse might be incorporated with minimum design change is as follows. The first pulse is a conventional 90° rf pulse, whose free induction decay is not recorded. After a variable interval τ_2, this pulse is followed by a 180° laser refocusing pulse, so that the nuclear magnetization is coherently reestablished to reach a maximum (the echo) at double the chosen interval.[35] At this point the data collection is initiated. The experiment is then repeated, as in the conventional method, with τ_2 incremented. This method is essentially the reverse of LASEI, because its key feature is a conventional 90° rf pulse followed by a 180° laser pulse. Of basic scientific

interest in this type of experiment would be the first experimental demonstration that a 180° laser pulse can refocus nuclear spins to produce an echo whose extent would depend on the laser-induced flip angle θ, so that the echo is maximized for a flip angle of exactly 180°. However, there should be an echo present with any flip angle, because the laser is always being used to rebuild magnetization to some measurable extent. In this type of experiment the refocusing effectively introduces high resolution[41] and this would be the role played by the laser.

Whenever a 180° radio-frequency pulse is used in contemporary NMR technology (which is mature and highly developed), it can be replaced in principle by a circularly polarized laser pulse. Among many applications would be the use of a laser pulse in the conventional technology[35] used in creating multiple-quantum coherence, for example, double and triple quantum correlated spectroscopy. Another example in which a 180° rf pulse can be replaced by a 180° laser pulse is INEPT,[35] the technique in which insensitive nuclei are enhanced by polarization transfer. Here the 180° laser pulse would be sandwiched between two conventional 90° rf pulses. Yet another possibility is the use of a 180° laser pulse in the Müller sequence[35, 41] in proton-detected COSY experiments. These are more advanced pulse designs, however; the simplest experiment is the LASEI sequence, which at this early stage would be important in demonstrating for the first time the ability of a laser pulse to generate free induction decay, i.e., to produce nuclear magnetization through the $\mathbf{B}_{\Pi}$ vector, a magnetization that decays characteristically with time after the laser pulse has passed through the sample. The rate of decay can be orders of magnitude slower, and the characteristic longitudinal decay time T_1 orders of magnitude longer, than the pulse duration.

APPENDIX A: SENSE OF ROTATION AND HANDEDNESS OF AN ELECTROMAGNETIC PLANE WAVE

In this appendix we stress the difference between the handedness and the sense of rotation of an electromagnetic plane wave. The subscripts R and L in Eqs. (6), (7), and (38), for example, refer to sense of rotation, i.e., leftwise or rightwise of the rotating vectors $\mathbf{E}$ and $\mathbf{B}$. Thus, $\boldsymbol{\kappa}_L$ should be read as "the linear momentum of a photon whose sense of rotation is leftwise," i.e., has a left state of spin, corresponding to the well-known photon quantum number $M_S = +1$. The spin of the photon is intrinsic and unremovable from fundamental postulate, and the parity operator P cannot change the sense of this or any other spin, i.e., cannot change the spin of the photon's angular velocity vector. Therefore, in this notation

$$P(\boldsymbol{\kappa}_L) = -\boldsymbol{\kappa}_L \tag{A.1}$$

because the direction of linear momentum of the photon is changed by P, but the leftwise sense of spin is not.

Clearly, the subscript L must be understood to signify the sense of spin of the photon. The handedness of the photon can be thought of as the product of the photon's linear and angular velocities, and the handedness operator $\hat{H}$ of the text is the product

$$\hat{H}(\mathbf{v}\boldsymbol{\omega}) = P(\mathbf{v})P(\boldsymbol{\omega}) = -(\mathbf{v}\boldsymbol{\omega}) \tag{A.2}$$

Therefore, the handedness operator can be thought of as equivalent to two parity operations, the product (A.2).

The existence of a left- and right-spinning photon with respect to the direction of its propagation implies, inter alia, the existence[31] of left and right circularly polarized electromagnetic plane waves, this being a type of particle/wave duality. It follows that the P operator cannot change the sense of rotation of the tip of a vector such as $\mathbf{E}$ which traces out a circle[36] in a fixed plane perpendicular to the direction of propagation of the plane wave. Thus,

$$\mathbf{E}_L = E_0(\mathbf{i} + \mathrm{i}\mathbf{j})\exp[-\mathrm{i}(\omega t - \boldsymbol{\kappa}_L \cdot \mathbf{r})] \tag{A.3}$$

means a left rotating plane wave in our notation, propagating in $+\boldsymbol{\kappa}_L$. The P operator changes $\boldsymbol{\kappa}_L$ to $-\boldsymbol{\kappa}_L$ and produces a left rotating plane wave propagating in $-\boldsymbol{\kappa}_L$. The handedness operator $\hat{H}$ produces a right rotating $\mathbf{E}$ vector propagating in $+\boldsymbol{\kappa}_R$.

Therefore, we prefer to make a distinction between the parity operator P and the handedness operator $\hat{H}$ when dealing with electromagnetic plane waves or, equivalently, photons. We emphasize that the subscripts L and R must be understood to mean "rotating leftwise or rightwise" throughout this chapter and in related articles in the literature,[14-20] and that they do *not* mean "left-handed" or "right-handed." This is a subtle but fundamentally important distinction.

Note that the motion reversal operator T must reverse the sense of any motion, and so must reverse the sense of spin of a photon or the sense of rotation of a vector such as $\mathbf{E}$ in its equivalent electromagnetic plane wave. Also, T must reverse the linear momentum of the photon, and so must also reverse the sign of the propagation vector κ in the plane wave equivalent to the photon. So

$$T(\boldsymbol{\kappa}_L) = -\boldsymbol{\kappa}_R \tag{A.4}$$

and it follows that[19]

$$T(\mathbf{E}_L) = \mathbf{E}_R^* \text{ etc.} \tag{A.5}$$

as in the text. The handedness of the photon or wave is unaffected by the T operator, because the latter reverse both the sense of rotation and direction of propagation simultaneously:

$$T(\boldsymbol{\nu})T(\boldsymbol{\omega}) = +(\boldsymbol{\nu}\boldsymbol{\omega}) \tag{A.6}$$

APPENDIX B: DEVELOPMENT OF THE SECOND-ORDER INTERACTION ENERGY

In this appendix we show that the second-order electronic interaction energy $i\boldsymbol{\alpha}'' \cdot \boldsymbol{\Pi}^{(A)}$ can be rewritten as a term quadratic in $\mathbf{B}_\Pi$ and proportional to the paramagnetic electronic susceptibility $\boldsymbol{\chi}''$, a T-negative, P-positive axial vector. This demonstrates clearly that $i\boldsymbol{\alpha}'' \cdot \boldsymbol{\Pi}^{(A)}$ is a term describing an induced electronic magnetic dipole moment multiplied by the square of $\mathbf{B}_\Pi$.

The first steps are

$$\begin{aligned} E_4 &= i\boldsymbol{\alpha}'' \cdot \boldsymbol{\Pi}^{(A)} \\ &= -(2|\boldsymbol{\alpha}''|cB_0\mathbf{k}) \cdot (cB_0\mathbf{k}) \\ &= -2|\boldsymbol{\alpha}''|c^2\mathbf{B}_\Pi \cdot \mathbf{B}_\Pi \end{aligned} \tag{B.1}$$

where $|\boldsymbol{\alpha}''|$ is the magnitude of the axial vector $\boldsymbol{\alpha}''$, and $\mathbf{k}$ is a unit axial vector as in the text.

The sequence (B.1) shows immediately that E_4 is quadratic in $\mathbf{B}_\Pi$, so that the quantity $2|\boldsymbol{\alpha}''|c^2$ must have the units of electronic magnetic susceptibility,[36] denoted

$$\chi_{ij} = \chi'_{ij} + i\chi''_{ij} \tag{B.2}$$

It is well established[36] that the imaginary part χ''_{ij} is a T-negative, P-positive, rank two polar tensor, which by fundamental tensor algebra is also an axial vector:

$$\boldsymbol{\chi}'' \equiv \chi''_i = \varepsilon_{ijk}\chi''_{jk} \tag{B.3}$$

It follows by symmetry that

$$|\boldsymbol{\chi}''| = 2\zeta|\boldsymbol{\alpha}''|c^2 \tag{B.4}$$

where ζ is a T- and P-positive unitless scalar. Thus,

$$E_4 = -\frac{|\boldsymbol{\chi}''|B_\Pi^2}{\zeta} = -\frac{|\boldsymbol{\chi}''|B_0^2}{\zeta} \tag{B.5}$$

where $|\boldsymbol{\chi}''|$ is the magnitude of the vector $\boldsymbol{\chi}''$. Comparing (B1) and (B4) yields

$$i\boldsymbol{\alpha}'' \cdot \boldsymbol{\Pi}^{(A)} = -\frac{|\boldsymbol{\chi}''|B_0^2}{\zeta} \tag{B.6}$$

This relation provides several insights to the meaning of the term $i\boldsymbol{\alpha}'' \cdot \boldsymbol{\Pi}^{(A)}$, which on first sight may appear to some readers to be abstract.

1. E_4 is simply an energy of interaction of $\mathbf{B}_\Pi$ with a laser-induced electronic magnetic dipole moment of magnitude

$$|\mathbf{m}^{(\mathrm{ind})}| = |\boldsymbol{\chi}''|B_0/\zeta \tag{B.7}$$

where $|\boldsymbol{\chi}''|$ is the magnitude of the sample's electronic paramagnetic susceptibility, a molecular property tensor defined from time-dependent second-order perturbation theory[31, 36]:

$$\begin{aligned} \chi''_{\alpha\beta} = -\chi''_{\beta\alpha} = -\frac{2}{\hbar}\sum_{j\neq n}\frac{\omega}{\omega_{jn}^2 - \omega^2} \\ \times \mathrm{I_m}\left(\langle n|\hat{m}_\alpha|j\rangle\langle j|\hat{m}_\beta|n\rangle\right) \end{aligned} \tag{B.8}$$

where ω_{jn} is a transition frequency between states n and j, and ω is the frequency of the electromagnetic radiation, i.e., the frequency that appears in $\mathbf{E}$ and $\mathbf{E}^*$. In Eq. (B.8) $\hat{m}_\alpha$ and $\hat{m}_\beta$ are magnetic dipole moment operators.

From Eq. (B.1),

$$i\boldsymbol{\Pi}^{(A)} \cdot \mathbf{k} = 2c^2\mathbf{B}_\Pi \cdot \mathbf{B}_\Pi \tag{B.9}$$

where $\mathbf{k}$ is a unit axial vector, meaning that

$$i|\mathbf{E} \times \mathbf{E}^*| = 2c^2\mathbf{B}_\Pi \cdot \mathbf{B}_\Pi \tag{B.10}$$

This shows that the vector cross product of $\mathbf{E}$ with $\mathbf{E}^*$ is proportional to the vector dot product of $\mathbf{B}_\Pi$ and $\mathbf{B}_\Pi$.

2. Using the relations

$$\mathbf{B}_{\Pi} = \nabla \times \mathbf{A}_{\Pi} \tag{B.11}$$

and the vector identity

$$(\mathbf{F} \times \mathbf{G}) \cdot (\mathbf{H} \times \mathbf{I}) = (\mathbf{F} \cdot \mathbf{H})(\mathbf{G} \cdot \mathbf{I}) - (\mathbf{F} \cdot \mathbf{I})(\mathbf{G} \cdot \mathbf{H}) \tag{B.12}$$

gives

$$\mathbf{E}_4 = -2|\boldsymbol{\alpha}''|_c^2 \nabla^2 A_{\Pi}^2 = -\frac{|\boldsymbol{\chi}''|}{\zeta} \nabla^2 A_{\Pi}^2 \tag{B.13}$$

which brings out a formal similarity with Eq. (41) of the text. However, Eq. (B.13) refers to a T-negative, P-positive, paramagnetic susceptibility vector, while Eq. (41) relates[31] to a T-positive, P-positive, symmetric, diamagnetic, polar susceptibility tensor of rank two, the real part of χ_{ij} of Eq. (B.2), a tensor that does not have a rank one vector equivalent. Note that in Eq. (B.13), ∇^2 operates on A_{Π}^2, while in Eq. (41), A_{Π}^2 is not operated upon. We have

$$\nabla^2 = \nabla \cdot \nabla = \frac{\partial^2}{\partial X^2} + \frac{\partial^2}{\partial Y^2} + \frac{\partial^2}{\partial Z^2} \tag{B.14}$$

and, self-consistently,

$$\nabla^2 A_{\Pi}^2 = B_{\Pi}^2 = B_0^2 \tag{B.15}$$

3. Finally, from semiclassical, time-dependent, second-order perturbation theory,[36]

$$\alpha''_{\alpha\beta} = -\alpha''_{\alpha\beta} = -\frac{2}{\hbar} \sum_{j \neq n} \frac{\omega}{\omega_{jn}^2 - \omega^2} \mathrm{Im}\left(\langle n|\hat{\mu}_{\alpha}|j\rangle\langle j|\hat{\mu}_{\beta}|n\rangle\right) \tag{B.16}$$

where $\hat{\mu}$ are electric dipole moment operators. This shows that

$$\boldsymbol{\chi}'' \propto (\text{Velocity})^2 \boldsymbol{\alpha}'' \tag{B.17}$$

because an electric dipole moment has the units of charge times distance, and magnetic dipole moment has the units of charge times distance times linear velocity.[31] This is consistent with Eq. (B.4) because c has the units of velocity, and ζ is unitless.

Therefore, the $\mathbf{B}_{\Pi}$ concept leads to a self-consistent development of the energy E_4, and to a simple physical interpretation, Eq. (B.4).

APPENDIX C: RELATING THE $\mathbf{B}_{\Pi}$ VECTOR TO FUNDAMENTAL ELECTROMAGNETIC QUANTITIES

It is well known[36] that the polarization state of a monochromatic electromagnetic plane wave can be described in terms of the four, real, scalar Stokes parameters. Of particular interest is the third Stokes parameter S_3, defined by

$$S_3 = -\mathrm{i}(E_X E_Y^* - E_Y E_X^*) \tag{C.1}$$

which is none other than the magnitude of the conjugate product vector $\mathbf{\Pi}^{(A)}$ of the text. It follows immediately that

$$\mathbf{\Pi}^{(A)} = \mathrm{i}S_3\mathbf{k} = \mathrm{i}\left(\frac{8I_0c}{\varepsilon_0}\right)^{1/2} (\pm\mathbf{B}_{\Pi}) \tag{C.2}$$

an equation that defines $\mathbf{B}_{\Pi}$ in terms of the well-known S_3 of fundamental electromagnetic theory.

This is a useful link because S_3 is well defined in terms of polarization properties. For example,

$$S_3 = 2E_0^2 \sin 2\eta \tag{C.3}$$

where η is the ellipticity of the plane wave. For circular polarization, $\eta = \pm\pi/4$. The ellipticity can be conversely related to S_3 by[36]

$$\eta = \frac{1}{2}\tan^{-1}\left[\frac{S_3}{(S_1^2 + S_2^2)^{1/2}}\right] \tag{C.4}$$

Furthermore, if $I(\sigma, \tau)$ denotes the intensity of light transmitted through a retarder which subjects the Y component to a retardation τ with respect to the X component, followed by an analyzer with its transmission axis oriented at an angle σ to the X axis, then

$$S_3 \propto I\left(\frac{3\pi}{4}, \frac{\pi}{2}\right) - I\left(\frac{\pi}{4}, \frac{\pi}{2}\right) \tag{C.5}$$

so that S_3 is the excess in intensity transmitted by a device that accepts

right circularly polarized light over one that accepts left circularly polarized light.[36] This shows that an excess of circular polarization is needed to produce $\mathbf{B}_{\Pi}$ in a laser beam, as in the text. $\mathbf{B}_{\Pi}$ is maximized if the beam is fully left or right circularly polarized, because S_3 is maximized. S_3 vanishes in linear polarization and so does $\mathbf{B}_{\Pi}$.

The polarization state of a light beam can also be defined by a matrix[36]:

$$\rho_{\alpha\beta} = \frac{E_\alpha E_\beta^*}{E_0^2} \tag{C.6}$$

with scalar elements. This is a Hermitian polarization density matrix, or a coherency matrix, the off-diagonals of which contain S_3:

$$\rho_{\alpha\beta} = \frac{1}{2S_0}\begin{bmatrix} S_0 + S_1 & -S_2 + iS_3 \\ -S_2 - iS_3 & S_0 - S_1 \end{bmatrix} \tag{C.7}$$

Clearly, this leads to Eq. (C.1) because the off-diagonals contain iS_3 and $-iS_3$. It follows that the off-diagonal elements of the coherency matrix of a plane wave also contain the magnitude of the vector $\mathbf{B}_{\Pi}$, because this magnitude is simply proportional to S_3. The coherency matrix is a second-rank spinor,[36] a real four-dimensional vector in a complex two-dimensional space. The components of the vector are related to the four Stokes parameters, and the coherency matrix is analogous with a density matrix in quantum mechanics. An incoherent superposition of pure quantum-mechanical states is a mixed quantum-mechanical state[36] must be represented by a density matrix. These analogies are useful for the demonstration of the existence of $\mathbf{B}_{\Pi}$ in rigorous quantum field theory, relativistic electrodynamics, and gauge theory. It is also clear that $\mathbf{B}_{\Pi}$ has a rigorous definition in stochastic electrodynamics, as discussed in several articles of this book.

In quantum optics, the third Stokes parameter S_3 (Ref. 48) becomes a Hermitian operator, $\hat{S}_3$, and the electric field vector becomes an operator ($\hat{E}$) of the electromagnetic field, being proportional to an annihilation operator, labeled $\hat{a}_+$ or $\hat{a}_-$ according to the sense of polarization.[48] In this notation, the third Stokes operator can be shown to be the difference

$$\hat{S}_3 = \hat{a}_+^+\hat{a}_+ - \hat{a}_-^+\hat{a}_- \tag{C.8}$$

where the annihilation operators satisfy the commutation relation

$$\left[\hat{a}_+, \hat{a}_+^+\right] = \delta_{++} \tag{C.9}$$

The quantum-field Stokes operators themselves obey a commutation law:

$$\left[\hat{S}_1, \hat{S}_2\right] = 2i\hat{S}_3 \tag{C.10}$$

and the classical third Stokes parameter S_3 is the expectation value of the quantum-field operator $\hat{S}_3$. In Cartesian coordinates we have

$$\hat{a}_\pm = \frac{1}{\sqrt{2}}\left(\hat{a}_X \mp i\hat{a}_Y\right) \tag{C.11}$$

In the quantum electromagnetic field of a laser, therefore, the $\mathbf{B}_{\Pi}$ vector becomes an operator proportional to the third Stokes $\hat{S}_3$, i.e., $\mathbf{B}_{\Pi}$ can be quantized, unlike a conventional flux density vector generated by a magnet.

A coherent eigenstate of the quantum field can be defined with respect to the annihilation operator â by[48]

$$\hat{a}|\alpha\rangle = \alpha|\alpha\rangle \tag{C.12}$$

and it can be shown[48] that $|\alpha|^2$ is a mean number of photons in the quantum field. The classical third Stokes parameter S_3 is the expectation value

$$S_3 = \langle\alpha|\hat{S}_3(Z)|\alpha\rangle \tag{C.13}$$

which can be written[48] as

$$S_3 = |\alpha_+|^2 - |\alpha_-|^2 \tag{C.14}$$

which is a difference in the mean number of photons in the + circular mode of the operator $\hat{E}_+$ and the − circular mode.

It follows that the classical $\mathbf{B}_{\Pi}$ vector is an expectation value of the quantized $\hat{\mathrm{B}}_{\Pi}$ operator:

$$\mathbf{B}_{\Pi} = \langle\alpha|\hat{B}_{\Pi}(Z)|\alpha\rangle \tag{C.15}$$

The number of photons in these circular modes are constants[48] of the motion, which implies inter alia that $\hat{B}_{\Pi}$ is frequency independent. Therefore, $\mathbf{B}_{\Pi}$ has a clearly defined meaning in quantum-field theory, and is generated in general by an electromagnetic field that is made up of photons, i.e., is quantized. This is yet another form of particle wave duality.

Finally, it is interesting to note that the Heisenberg uncertainty principle can be expressed in terms of[48]

$$\left(\left\langle\left(\Delta\hat{S}_1\right)^2\right\rangle\left\langle\left(\Delta\hat{S}_2\right)^2\right\rangle\right)^{1/2} \geq |\langle\hat{S}_3\rangle| \tag{C.16}$$

and is fundamentally dependent, therefore, on the existence of the quantum-field operator $\hat{B}_\Pi$.

APPENDIX D: SIMPLE PHYSICAL PROPERTIES OF THE $\mathbf{B}_\Pi$ VECTOR

In this appendix we discuss a few simple physical properties expected of the $\mathbf{B}_\Pi$ vector. Because $\mathbf{B}_\Pi$ is a static, uniform, magnetic field an electronic charge in $\mathbf{B}_\Pi$ will move (classically) along a helix under the influence of $\mathbf{B}_\Pi$, a helix having its axis along the direction of the magnetic field with a radius r. The linear velocity of the electron would be constant. There is a striking similarity between the motion of the electron in $\mathbf{B}_\Pi$ and the motion of the tip of the $\mathbf{E}$ vector of a circularly polarized laser. The tips of the $\mathbf{E}$ vectors at a given instant distributed along the direction of propagation of a circularly polarized light beam form[36] a helix that moves along the direction of propagation but does not rotate. An electronic charge will follow the same pattern of motion (because the force on the electron is $e\mathbf{E}$), and as the helix moves through space, the electronic charge e rotates in a plane according to the sense of rotation (Appendix A). This examination of the motion of an electron in a circular polarized laser shows that the $\mathbf{B}_\Pi$ vector is closely connected with the rotational motion of the $\mathbf{E}$ vector of the laser (Appendix B).

If the $\mathbf{B}_\Pi$ vector is spatially inhomogeneous, specifically, if its magnitude varies in the Z axis of the laser's propagation, the inhomogeneity is expected to lead to a slow transverse drift of the guiding center of the helical trajectory of an electron placed in the field. Since the magnitude of $\mathbf{B}_\Pi$ is directly proportional to the square root of the laser's intensity by Eq. (14), a gradient $\partial\mathbf{B}_\Pi/\partial Z$ can be established by varying the laser's intensity along the direction of propagation Z. This is accomplished experimentally by expanding or focusing the beam. If a beam of electrons (or atoms such as silver) is directed at a target in the same axis Z, colinear with the expanding or focused laser beam, we expect a deflection of the electron or atom beam by the gradient $\pm\partial\mathbf{B}_\Pi/\partial Z$ of the laser, in direct analogy with the well-known Stern-Gerlach experiment. In order to detect the deflection, it is an advantage to make $\partial\mathbf{B}_\Pi/\partial Z$ as large as possible, and this can

be accomplished by pulsing the laser and using a fast detector system, readily available from contemporary technology. As in the original Stern-Gerlach experiment, such a deflection shows the existence inter alia of electronic spin and the gradient $\partial\mathbf{B}_\Pi/\partial Z$ of a focused or expanded laser beam. Unlike the original Stern-Gerlach experiment, however, the gradient $\partial\mathbf{B}_\Pi/\partial Z$ is quantized, as discussed in Appendix C.

In classical electrodynamics, $\mathbf{B}_\Pi$ is a uniform magnetostatic field and, formally, there must be a source of this field located at infinity. This source may be an electric current density or magnetic charge density. However, since $\mathbf{B}_\Pi$ is created by a circularly polarized electromagnetic field, the source of $\mathbf{B}_\Pi$ and the source of the electromagnetic field must be the same. This implies that the classical $\mathbf{B}_\Pi$ vector exists in the absence of charges, because a classical electromagnetic field exists in the absence of charges, and thus propagates in vacuo. In Appendix C we saw that $\mathbf{B}_\Pi$ is the expectation value of an operator $\hat{B}_\Pi$ proportional to the third Stokes operator of the quantized electromagnetic field: thus, $\mathbf{B}_\Pi$ is clearly defined in terms of photons. It follows that the source of $\mathbf{B}_\Pi$ is the same as the source of these pohtons, and is therefore well defined. The classical magnetostatic $\mathbf{B}_\Pi$ is an expectation value of a quantized electromagnetic field operator $\hat{B}_\Pi$ directly proportional to the third Stokes operator.

APPENDIX E: THE QUANTIZED $\hat{B}_\Pi$

In this appendix quantum-field theory is used to show that a beam of N photons generates quantized static magnetic flux density ($\hat{B}_\Pi$), defined by the operator equation

$$\hat{B}_\Pi = B_0\frac{\hat{J}}{\hbar} \tag{E.1}$$

where B_0 is the scalar magnetic flux density amplitude (tesla) of the beam and $\hat{J}$ is the intrinsic angular momentum operator of one photon. The operator $\hat{B}_\Pi$ is related directly to the angular momentum operator $\hat{J}$ of the photon.

Here $\hat{B}_\Pi$ is the quantum-field description of the classical $\mathbf{B}_\Pi$ vector. Equation (E.1) appears to be a new fundamental property of photons, indicating immediately the existence of $\hat{B}_\Pi$ given that of $\hat{J}$. Clearly, $\hat{J}$ and $\hat{B}_\Pi$ are zero only if the (laser) beam of N photons has no element of coherent circular polarity (e.g., if it is linearly polarized).

The transition from classical to quantized field theory is made through the third Stokes operator $\hat{S}_3$, recently introduced by Tanaś and Kielich[48]:

$$\hat{S}_3 = -\left(\frac{2\pi\hbar\omega}{n^2(\omega)V}\right)i\left(\hat{a}_X^+\hat{a}_Y - \hat{a}_Y^+\hat{a}_X\right) \tag{E.2}$$

Here $n(\omega)$ is the refractive index, V is the quantization volume, and $\hat{a}^+$ and $\hat{a}$ denote respectively the creation and annihilation operators. Defining a coherent state of a beam of N photons by the Schrödinger equation[48]

$$\hat{a}|\alpha\rangle = \alpha|\alpha\rangle \tag{E.3}$$

provides the expectation value

$$\langle\alpha|\hat{S}_3|\alpha\rangle = |\alpha_+|^2 - |\alpha_-|^2 \tag{E.4}$$

with

$$\alpha_+ = \frac{1}{\sqrt{2}}(\alpha_X \mp i\alpha_Y) \tag{E.5}$$

We define the operator

$$\hat{B}_\Pi \equiv \left(\frac{\varepsilon_0}{8I_0c}\right)^{1/2}\hat{S}_3 \tag{E.6}$$

and arrive at the equation

$$\hat{B}_\Pi = \left(\frac{\varepsilon_0}{8I_0c}\right)^{1/2}\left(\frac{2\pi\omega}{n^2(\omega)V}\right)\hbar\left(\hat{a}_+^+\hat{a}_+ - \hat{a} \pm \hat{a}_-\right) \tag{E.7}$$

with

$$\hat{a}_\pm = \frac{1}{\sqrt{2}}(\hat{a}_X \mp i\hat{a}_Y) \tag{E.8}$$

The quantity

$$\hbar\left(\hat{a}_+^+\hat{a}_+ - \hat{a}_-\hat{a}_-\right) \equiv \hbar(\hat{n}_+ - \hat{n}_-) \tag{E.9}$$

has the units of quantized angular momentum because $(\hat{n}_+ - \hat{n}_-)$ is dimensionless. Here

$$\begin{aligned}\hat{n}^+ &= \hat{a}_+^+\hat{a}_+ \\ \hat{n}^- &= \hat{a}_-^+\hat{a}_-\end{aligned} \tag{E.10}$$

are the number of photons operators.[48]

We know that the total angular momentum of a beam of N photons propagating in Z is $NM_J\hbar$, where M_J is the azimuthal quantum number associated with $\hat{J}$. Defining the angular momentum eigenfunction of a single photon by $|JM_J\rangle$ we arrive at the Schrödinger equation:

$$\hbar(\hat{n}_+ - \hat{n}_-)|JM_J\rangle = \hbar NM_J|JM_J\rangle \tag{E.11}$$

From (E.7) in (E.11)

$$\frac{n^2(\omega)V}{2\pi\omega}\hat{S}_3|JM_J\rangle = \hbar NM_J|JM_J\rangle \tag{E.12}$$

and with the identity

$$\hat{J} = \left[\frac{n^2(\omega)V}{2\pi\omega N}\right]\hat{S}_3 \tag{E.13}$$

Eq. (E.12) becomes the standard Schrödinger equation describing the angular momentum of one photon:

$$\hat{J}|JM_J\rangle = \hbar M_J|JM_J\rangle \tag{E.14}$$

From (E.6) and (E.13)

$$\hat{B}_\Pi = \left(\frac{\varepsilon_0}{8I_0c}\right)^{1/2}\left[\frac{2\pi\omega N}{n^2(\omega)V}\right]J \equiv \zeta\hat{J} \tag{E.15}$$

showing that $\hat{B}_\Pi$ is directly proportional to $\hat{J}$. Considerable insight to the nature of the constant ζ is obtained with the results of Tanaś and Kielich[48]:

$$\begin{aligned}S_0 &= \frac{2\pi\omega\hbar}{n^2(\omega)V}\langle\alpha|\hat{S}_0|\alpha\rangle \\ \langle\alpha|\hat{S}_0|\alpha\rangle &= N\end{aligned} \tag{E.16}$$

where $\hat{S}_0$ is the zeroth Stokes operator, and S_0 is the zeroth Stokes parameter. Furthermore, we make use of the classical result[36]

$$S_0 = 2E_0^2 \tag{E.17}$$

From (E.16) and (E.17)

$$E_0^2 = \frac{\pi\omega\hbar N}{n^2(\omega)V} \tag{E.18}$$

Using (E.18) in (E.15) gives, finally, the fundamental and simple operator equation

$$\hat{B}_\Pi = B_0\left(\frac{\hat{J}}{\hbar}\right) \tag{E.19}$$

It is clear that Eq. (E.19) defines $\hat{B}_\Pi$ simply and directly in terms of $\hat{J}$, the angular momentum operator of one photon. It follows that

$$\hat{B}_{\Pi Z}|JM_J\rangle = B_0 M_J|JM_J\rangle \tag{E.20}$$

so that the expectation value of the Z component of $\hat{B}_\Pi$ is B_0M_J. It appears that there are many implications of this result, in principle, a few of which are as follows.

1. A beam of N photons propagating in Z generates the magnetic field B_0M_J, whose classical value is $\pm B_0\mathbf{k}$.
2. This magnetic field forms a scalar interaction energy with any quantized magnetic dipole moment, nuclear or electronic, and this is the basis of optical NMR and ESR.[33]
3. Conventionally,[31] a right-handed photon carries the minimum intrinsic angular momentum $M_J = -1$, and the left photon $M_J = +1$. However, a photon's M_J can exceed unity.[31]
4. Since $\hat{J}$ is an intrinsic, unremovable property of the photon, then $\hat{B}_\Pi$ is an intrinsic, unremovable property of the beam of N photons.
5. It follows that a circularly polarized beam of N photons must always generate $\hat{B}_\Pi$, which invariably forms a scalar interaction energy with a quantized magnetic dipole moment operator following the theory of angular momentum coupling.[21]

6. Finally, whenever a static magnetic field is used experimentally, it is also possible, in principle, to use a circularly polarized laser beam, at any frequency, from radio frequencies to those of gamma rays. The magnitude of the classical $\mathbf{B}_\Pi$ can be estimated from the simple equation (14).

Acknowledgments

The Leverhulme Trust is thanked for a Fellowship for the development of optical resonance techniques, and Rex Richards, F.R.S., for correspondence. The Cornell Theory Center is ackowledged for additional support, and the Materials Research Laboratory of Penn State University for the award of a Visiting Senior Research Associateship. Correspondence and many interesting discussions are acknowledged with Warren S. Warren and colleagues at Princeton, Jack L. Freed and Keith A. Earle at Cornell, Stanisław Kielich at Poznań, Ray Freeman, F.R.S., at Cambridge, and Laurence Barron at Glasgow. Richard Ernst is thanked for a seminar invitation to ETH, Zürich, and for interesting and positive discussions on the optical resonance ideas presented in this article.

References

1. P. S. Pershan, *Phys. Rev. A* **130**, 919 (1963).
2. Y. R. Shen, *Phys. Rev. A* **134**, 661 (1964).
3. J. P. van der Ziel, P. S. Pershan, and L. D. Malmstrom, *Phys. Rev. Lett.* **15**, 190 (1965).
4. P. S. Pershan, J. P. van der Ziel, and L. D. Malmstrom, *Phys. Rev.* **143**, 574 (1966).
5. S. Kielich, *Proc. Phys. Soc.* **86**, 709 (1965).
6. S. Kielich, *Acta. Phys. Pol.* **29**, 875 (1966); **30**, 851 (1966).
7. P. W. Atkins and M. H. Miller, *Mol. Phys.* **15**, 503 (1968).
8. N. L. Manakov, V. D. Ovsiannikov, and S. Kielich, *Acta Phys. Pol.* **A53**, 581 (1978).
9. N. L. Manakov, V. D. Ovsiannikov, and S. Kielich, *Acta Phys. Polon.* **A53**, 595 (1978).
10. N. L. Manakov, V. D. Ovsiannikov, and S. Kielich, *Acta Phys. Polon.* **A53**, 737 (1978).
11. B. L. Silver, *Irreducible Tensor Methods*, Academic, New York, 1976.
12. R. Zare, *Angular Momentum*, Wiley Interscience, New York, 1984.
13. C. P. Slichter, *Principles of Magnetic Resonance*, 2nd ed., Springer, Berlin, 1978.
14. M. W. Evans, *Phys. Rev. Lett.* **64**, 2909 (1990).
15. M. W. Evans, *Opt. Lett.* **14**, 863 (1990).
16. M. W. Evans, *Phys. Lett. A* **146**, 475 (1990); **147**, 364 (1990).
17. M. W. Evans, *J. Mol. Spectrosc.* **143**, 327 (1990); **146**, 351 (1991).
18. M. W. Evans, *Physica B*, **168**, 9 (1991).
19. M. W. Evans, in I. Prigogine and S. A. Rice (Eds.), *Advances in Chemical Physics*, Vol. 81, Wiley Interscience, New York, 1992, pp. 361–702.
20. M. W. Evans, *Phys. Lett. A* **146**, 185 (1990).
21. A. R. Edmonds, *Angular Momentum in Quantum Mechanics*, 2nd ed., Princeton University Press, Princeton, NJ, 1960.
22. M. W. Evans, *Physica B*, **179**, 237 (1992).
23. M. W. Evans, *Physica B*, **182**, 118 (1992).

24. M. W. Evans, *J. Phys. Chem.* **95**, 2256 (1991).
25. M. W. Evans, *Chem. Phys.* **157**, 1 (1991).
26. M. W. Evans, *Physica B*, **182**, 227 (1992).
27. M. W. Evans, *Physica B*, **176**, 254 (1992).
28. M. W. Evans, *Physica B*, **182**, 237 (1992).
29. M. W. Evans, *Physica B*, **183**, 103 (1993).
30. M. W. Evans, *Physica B*, **179**, 157 (1992).
31. P. W. Atkins, *Molecular Quantum Mechanics*, 2nd ed., Oxford University Press, Oxford, UK, 1983.
32. D. Goswami, C. Hillegas, Q. He, J. Tull, and W. S. Warren, *Laser NMR Spectroscopy*, Proc. Exp. NMR Conference, St. Louis, Missouri, 8–12 April 1991.
33. W. S. Warren, S. Mayr, D. Goswami, and A. P. West, Jr., *Science*, **255**, 1683 (1992).
34. J. W. Akitt, *NMR and Chemistry: An Introduction to the Fourier Transform and Multinuclear Era*, 2nd ed., Chapman Hall, London, 1983.
35. S. W. Homans, *A Dictionary of Concepts in NMR*, Clarendon, Oxford, UK, 1989.
36. L. D. Barron, *Molecular Light Scattering and Optical Activity*, Cambridge University Press, Cambridge, UK, 1982.
37. M. W. Evans, *Int. J. Mod. Phys. B*, **5**, 1963 (1991), invited review.
38. M. W. Evans, *J. Mol. Liquids*, **48**, 77 (1991).
39. J. S. Griffith, *The Irreducible Tensor Method for Molecular Symmetry Groups*, Prentice Hall, Englewood Cliffs, NJ, 1962.
40. D. C. Hanna, M. A. Yuratich, and D. Cotter, *Nonlinear Optics of Free Atoms and Molecules*, Springer, New York, 1979.
41. R. R. Ernst, G. Bodenhausen, and A. Wokaun, *Principles of Nuclear Magnetic Resonance in One and Two Dimensions*, Oxford University Press, Oxford, UK, 1987.
42. R. R. Ernst and W. A. Anderson, *Rev. Sci. Instrum.* **37**, 93 (1966).
43. M. W. Evans, G. J. Evans, W. T. Coffey, and P. Grigolini, *Molecular Dynamics*, Wiley Interscience, New York, 1982.
44. J. Jortner, R. D. Levine, I. Prigogine, and S. A. Rice Eds., *Advances in Chemical Physics*, Vol. 47, Wiley Interscience, New York, 1981.
45. W. A. Molander, C. R. Stroud, Jr., and J. A. Yeazell, *J. Phys. B* **19**, L461 (1986).
46. M. W. Evans, S. Woźniak, and G. Wagnière, *Physica B* **173**, 357 (1991); **175**, 416 (1991).
47. S Kielich, in M. Davies (Senior Reporter), *Dielectric and Related Molecular Processes*, Vol. 1, Chem. Soc., London, 1972.
48. R. Tanaś and S. Kielich, *J. Mod. Opt.* **37**, 1935 (1990).

SOME PROPERTIES OF LONGITUDINAL FIELDS AND PHOTONS

M. W. EVANS*

Department of Physics, University of North Carolina, Charlotte, NC

CONTENTS

*Senior Visiting Research Associate, Materials Research Laboratory, Pennsylvania State University, University Park, PA 16802-4801; Visiting Scientist and Leverhulme Fellow, Cornell Theory Center, Ithaca, NY 14853.

Modern Nonlinear Optics, Part 2, Edited by Myron Evans and Stanisław Kielich. Advances in Chemical Physics Series, Vol. LXXXV.
ISBN 0-471-57546-1